MET.O.14

METEOROLOGICAL OFFICE
BOUNDARY LAYER RESEARCH BRANCH
TURBULENCE & DIFFUSION NOTE

T.D.N. No. 103

SEPARATION EFFECTS IN EKMAN LAYER FLOW OVER RIDGES

by

P.J.Mason & R.I.Sykes

February 1978

Separation effects in Ekman layer flow over ridges

P J Mason and R I Sykes

Met Office, Bracknell

(Received 10 February 1978)

Abstract

Two dimensional numerical integrations of the Navier Stokes equations for flow of an Ekman layer over a ridge on a range of length scales corresponding to large Rossby numbers are presented. The results are compared, where appropriate, with numerical solutions of the triple deck equations of boundary layer flow. For steady flow agreement is good and, as predicted by triple deck theory, the net change in total force on the domain is small for homogeneous flow. An increase in force arises either through gravity wave radiation, when triple deck predictions agree well, or when the ridge is sufficiently steep to give eddy shedding.

1. Introduction

Topography with horizontal length scales of the order of a few kilometres is often sufficiently steep to induce flow separation in the atmosphere. Such flows might well be expected to produce significant changes in the total momentum exchange between the atmosphere and the surface, but there has been little work on the topic. There have been a number of recent papers concerned with turbulent boundary layer flow over topography. Jackson and Hunt (1975) present a linear theory of turbulent flow over a small hill. Although this theory is limited to small perturbations, it is useful in interpreting numerical results such as those of Taylor (1977). Taylor's numerical work is mainly based on a transport equation for the turbulent kinetic energy, which together with a prescribed length scale gives an eddy viscosity. Any numerical model of a turbulent boundary layer is necessarily empirical, and the results are generally inaccurate in the case of strong perturbations such as separation bubbles. For this reason, Taylor has restricted most of his modelling to relatively shallow topography. An understanding of the corresponding laminar flow over a ridge would be very valuable in interpreting the turbulence model results, since it clarifies the distinction between basic dynamical processes and features due to the particular turbulence model utilised. Thus, as a preliminary step towards understanding atmospheric boundary layer separation over topography, we shall investigate the response of a laminar Ekman layer.

A recent development which has opened up research into boundary layer dynamics is the triple deck theory of Stewartson (1969), Messiter (1970), see Stewartson (1974) for a review. This theory incorporates an interaction between the boundary layer and the free stream, and permits the description of strong perturbations. This is in contrast to the classical boundary layer theory where the boundary layer responds entirely passively to external forcing. One major problem inherent in the passive (parabolic) boundary layer flows is the singularity at separation, Brown and Stewartson (1969), which prevents any useful description of separated flows by these methods. Smith (1977) has shown that separation within

the triple deck framework is a regular phenomenon, and that the triple deck structure is the correct description of the flow near the separation point. Smith (1973) was also first to apply the theory to flow over obstacles, although Hunt (1971) presents a similar, but incomplete, structure which is valid near the obstacle. These two studies of flow over ridges both contain linear analyses, but the non-linear equations of Smith (1973) have recently been solved numerically for separated flows by Sykes (1978).

The triple deck structure is valid in the limit of large Reynolds number, $R_e = U_0 \delta/\nu$, where U_0 is the free stream speed, δ the boundary layer thickness, and ν the kinematic viscosity. Whilst the triple deck is a consistent theory which has been successfully applied to a number of boundary layer phenomena, it still remains an asymptotic theory, and it is not possible to determine a priori how large the Reynolds number must be to obtain accurate results. Furthermore, when the hill dimensions do not satisfy the restrictions of the theory there will be loss of accuracy. In the case of the Ekman layer, there is another complication due to instabilities at Reynolds numbers greater than about 55 (Faller and Kaylor (1966), Lilly (1966)), which may prevent the triple deck giving any useful results. In view of the above difficulties, it is necessary to solve the complete Navier-Stokes equations to determine the actual flow.

In this paper we shall describe some numerical solutions of the Navier-Stokes equations for flow over topography. These results will be compared with some numerical solutions of the triple deck equations of motion. The effects of a stable stratification will also be investigated. Stratification effects were incorporated into the triple deck structure by Sykes (1978).

It will be shown that for small hills, the triple deck results are very similar to the Navier-Stokes solutions. Furthermore, for the smaller hills the Navier-Stokes solutions confirm the triple deck theory prediction that the net change in total momentum transfer is small; the pressure force on the hill is balanced by a reduction in the total viscous stress (Sykes 1978). Detailed analysis (Brighton 1978) shows that the relative increase in drag should be $O(\epsilon)$ and this is confirmed by the numerical results. In the case of ridges which are as high as the boundary layer depth, instabilities can be triggered which completely change the flow. These instabilities also have a dramatic effect on the total momentum transfer.

2. Outline of triple deck theory

In this section, we briefly describe the assumptions and structure of the triple deck. The reader is referred to Stewartson (1974) for a more detailed discussion. The theory is based on the small parameter $\epsilon = (U_0 \delta/\nu)^{-1/4}$, and is valid in the limit $\epsilon \to 0$. The triple deck, as its name suggests, is a flow structure with three different regions; each region has a horizontal length scale of order $\epsilon^{-1}\delta$, but differing vertical dimensions. The main deck is the undisturbed boundary layer scale, δ. In the triple deck interaction, a lower deck develops with a vertical scale of $\epsilon\delta$, and also an upper deck with a height scale of order $\epsilon^{-1}\delta$, ie the same as the horizontal scale.

This particular structure is determined by matching the order of magnitude of various terms in the Navier-Stokes equations. Some of the mystery of the length scales can be removed by supposing the topography has a length scale of $O(\chi\delta)$

and a height of $O(\varepsilon\delta)$, where ε and χ are to be determined from a balance of terms in the equations of motion. Since a laminar boundary layer has a linear velocity profile near the surface, the velocities in the vicinity of the hill will be $O(\varepsilon U_0)$. We require the triple deck to describe separated flows, so the perturbations must be of the same order as the basic velocities, hence the inertial and pressure gradient terms have magnitude $O(\varepsilon^2 U_0^2/\chi\delta)$. The viscous terms are $O(\nu U_0/\varepsilon\delta^2)$, therefore balancing these two quantities gives $\varepsilon^3\chi^{-1} = Re^{-1}$

A second relation between ε and χ is obtained from consideration of the flow at the top of the boundary layer. The boundary layer is flowing over a hill with slope $O(\varepsilon\chi^{-1})$, so the vertical velocities at the bottom of the upper deck will be $O(\varepsilon\chi^{-1}U_0)$. The pressure field will vary on a length scale of $O(\chi\delta)$ in the vertical, since in an inviscid interaction, neglecting effects such as stratification, there is no scale other than the horizontal one to determine the vertical structure. Now the essence of the triple deck is the interaction between the upper and lower decks via the pressure gradient. So, postulating the pressure perturbation to be $O(\varepsilon^2 U_0^2)$, the vertical pressure gradient in the upper deck is $O(\varepsilon^2 U_0^2/\chi\delta)$. This must balance the linearised vertical term in the vertual momentum equation, which is $O(\varepsilon^3 U_0^2/\chi^2\delta)$. Hence

$$\frac{\varepsilon^2 U_0^2}{\chi\delta} = \frac{\varepsilon U_0^2}{\chi^2\delta}$$

ie $\varepsilon = \chi^{-1}$

Thus $\varepsilon = Re^{-1/4}$, as anticipated. This argument is not a derivation of the triple deck, but illustrates its consistency, and the balances involved. The topography must be on a length scale of $\varepsilon^{-1}\delta$, and have a height of order $\varepsilon\delta$ in order to provoke a triple deck interaction, and then the topography will be entirely in the lower deck. This restriction on the size may seem to be a weakness of the theory. In fact, as far as boundary layer dynamics is concerned, this scale of topography is the most important, because the balance of terms ensure that all the forces, ie inertial, pressure, and viscous, are involved in the interaction, so that no essential effect is omitted.

We note at this stage that Brighton (1978) has shown that the variation of the

direction of the flow with height in the Ekman layer does not affect the triple deck equations in two-dimensions. The transverse velocity component is irrelevant because the triple deck length scale is too short for the Coriolis force to be effective.

Briefly, the dynamics of the triple deck are as follows. The lower deck flow satisfies the usual nonlinear boundary layer equations, ie parabolic equations driven by a pressure gradient (see §3(b)). This flow results in a streamline displacement at the top of the lower deck, which must match with the main deck flow. The main deck solution is then completely described by this displacement, ie the undisturbed boundary layer is simply displaced vertically throughout the main deck. The displacement depends only on the horizontal coordinate, and thus provides the lower boundary condition on the upper deck flow. The small perturbation generates a pressure field in the upper deck, where the flow is inviscid and linear. The horizontal pressure gradient at the bottom of the upper deck is precisely that which drives the lower deck.

Thus we have an interactive flow structure. The nonlinear lower deck equations are parabolic, and thus contain no upstream influence. However, the pressure gradient which drives this flow is related to the resultant streamline displacement via the elliptic upper deck flow, and this allows upstream influence.

3. Numerical models

(a) Navier-Stokes model

The numerical technique used to solve the Navier-Stokes equations with a curved boundary is described in Mason and Sykes (1978a). Briefly, the incompressible, Boussinesq equations of motion in the (x,z) - plane are

$$\frac{\partial u}{\partial t} + u\frac{\partial u}{\partial x} + w\frac{\partial u}{\partial z} = -\frac{\partial p}{\partial x} + fv + \frac{\partial}{\partial x}\left(2\nu_H \frac{\partial u}{\partial x}\right) + \frac{\partial}{\partial z}\left(\nu_0 \frac{\partial u}{\partial z} + \nu_H \frac{\partial w}{\partial x}\right)$$

$$\frac{\partial v}{\partial t} + u\frac{\partial v}{\partial x} + w\frac{\partial v}{\partial z} = -\frac{dP_0}{dy} - fu + \frac{\partial}{\partial x}\left(\nu_H \frac{\partial v}{\partial x}\right) + \frac{\partial}{\partial z}\left(\nu_0 \frac{\partial v}{\partial z}\right)$$

$$\frac{\partial w}{\partial t} + u\frac{\partial w}{\partial x} + w\frac{\partial w}{\partial z} = -\frac{\partial p}{\partial z} - \rho g + \frac{\partial}{\partial x}\left(\nu_0 \frac{\partial u}{\partial z} + \nu_H \frac{\partial w}{\partial x}\right) + \frac{\partial}{\partial z}\left(2\nu_0 \frac{\partial w}{\partial z}\right)$$

$$\frac{\partial \rho}{\partial t} + u\frac{\partial \rho}{\partial x} + w\frac{\partial \rho}{\partial z} = \frac{\partial}{\partial x}\left(\kappa_H \frac{\partial \rho}{\partial x}\right) + \frac{\partial}{\partial z}\left(\kappa_0 \frac{\partial \rho}{\partial z}\right)$$

$$\frac{\partial u}{\partial x} + \frac{\partial w}{\partial z} = 0$$

where (u, v, w) is the velocity vector in (x, y, z) coordinates, shown in figure 1. ρ is the relative perturbation density (the mean density is taken to be unity), f is the Coriolis parameter, g is the acceleration due to gravity, p is the pressure, and $\frac{dp_0}{dy}$ is the basic pressure gradient, responsible for the geostrophic wind in the x-direction. The diffusion terms require some explanation. ν_0 and K_0 are the kinematic viscosity and thermal diffusivity respectively, and describe diffusion in the vertical direction, while ν_H and K_H are diffusivities associated with horizontal derivatives. The equations are written in the above form to allow the use of artificial horizontal diffusion, which is necessary when using highly anisotropic grid spacings. The precise form of the viscous terms in the momentum equations is obtained from consideration of the form of the stress tensor, see Mason and Sykes (1978b). When $\nu_H = \nu_0$, the equations reduce to the usual form appropriate to an isotropic viscosity. The effects of different values of ν_H will be discussed in the next section.

The equations of motion are solved numerically on a rectangular Cartesian grid, with the usual staggered spacing of variables (see eg Piacsek and Williams 1970). Second-order accurate finite differencing is used for both time and space derivatives. The topography is included by setting velocities equal to zero below the surface, and making the viscous stress continuous across the solid boundary. Provided the first grid point above the surface is near enough to the surface, in a sense made more precise in Mason and Sykes (1978a), then the model is effectively second-order accurate everywhere. Essentially, the boundary layer must be resolved sufficiently well for the dynamics on the first grid point above the surface to be dominated by viscosity. It is also possible to solve the Poisson equation for the pressure in the entire rectangular domain, which allows the use of efficient solution methods.

Finally we discuss the boundary conditions on the system of equations. The lower surface is a no-slip boundary, ie $u = v = w = 0$, while the upper surface is stress-free, ie $\frac{\partial u}{\partial z} = \frac{\partial v}{\partial z} = w = 0$. In the horizontal direction,

periodic boundary conditions are specified. Apart from being simple to compute numerically, and well-posed mathematically, periodic boundary conditions are almost essential when attempting to estimate the total change in force on the lower boundary. This is because the viscous stress on the surface is reduced over long distances downstream, especially in strongly separated flows, and an extremely large integration domain would be necessary to include the full effect of the hill.

When stratification effects are included, the perturbation density on the surface of the topography is maintained at the value which would obtain at the same height in the undisturbed fluid. This minimises the effects of slope winds, induced by surface heating or cooling. The upper boundary is maintained at the initial temperature, but on the uppermost levels in the numerical model, a Rayleigh damping term is included in the equations. This is described in Mason and Sykes (1978b), and simulates an infinite fluid by absorbing gravity waves radiated by the topography, ie preventing any reflection.

(b) Triple deck model

The method used for the solution of the triple deck equations is described fully in Sykes (1978). The problem is to solve the two-dimensional boundary layer equations

$$u\frac{\partial u}{\partial x} + w\frac{\partial u}{\partial z} = -\frac{dp}{dx} + \frac{\partial^2 u}{\partial z^2}$$

$$\frac{\partial u}{\partial x} + \frac{\partial w}{\partial z} = 0$$

where (x, z), (u, w), and p are the dimensionless coordinates, velocity, and pressure respectively. The lower boundary condition is no-slip, while the upper boundary condition relates the streamline displacement to the pressure. This relationship is rather complicated and will not be presented here. Unfortunately, the upper boundary condition does not specify a local relationship, but is of elliptic type, ie involving values of the field at all points.

Thus, a streamline displacement is guessed, then the boundary layer equations are integrated numerically downstream, calculating the pressure field to satisfy the specified displacement. The upper boundary condition is then used to provide a new streamline displacement, and the whole process is repeated until the fields converge.

The method used to step the boundary layer equations (Sykes 1978) is a multi-step, mixed explicit implicit method.

There is some small oscillation of the velocity field in the flow reversal regions in the results presented below, but the oscillation does not grow downstream, and disappears as the grid length is reduced.

4. Results

In all the results from either the Navier-Stokes equation model or triple deck theory we have adopted a standard form of topography and relative size of domain. The height of the topography used is $S = h\cos^2\left(\frac{\pi x}{L}\right)$ for $|x| < L/2$ and $S = 0$ for $|x| \geq L/2$ where $4L$ is the total length of the periodic domain. This fixed type of topography and relative length of the domain is intended to help intercomparisons between various results. In general, longer domain lengths relative to the length of the topography are precluded if the numerical model is to adequately resolve the features of the flow. In all the results presented here L is sufficiently small to make rotation unimportant in the dynamics of the flow over the hill. (i.e. Rossby number, $U_0/fL \gg 1$).

We have presented the Navier-Stokes equation results in terms of atmospheric length and height scales and have used values of diffusion coefficient which are atmospherically reasonable. This has not been done on the pretext of simulating atmospheric flows, but rather, to elucidate what dynamical processes can occur in laminar flows on atmospheric scales. In our future work we plan to take a step nearer atmospheric reality by seeing how these processes are changed by the simulation of a turbulent boundary layer.

In all the Navier-Stokes results the depth of the domain has been fixed at 10 km. The vertical coefficient of diffusion ν_0 has been taken as 5 $m^2 S^{-1}$ and basic angular rotation speed $f/2$ as 0.00005 rad S^{-1} giving an Ekman boundary layer

depth $\delta = (2\nu_0/f)^{\frac{1}{2}} = 316m$. The basic pressure gradient in the y-direction $\frac{dP_0}{dy}$ has been fixed to give a basic geostrophic flow $U_0 = 10ms^{-1}$ which with the other parameters gives $\varepsilon = 0{\cdot}2$ (except for one of the triple deck comparisons in which $U_0 = 40ms^{-1}$ and $\varepsilon = 0{\cdot}14$). The component of the undisturbed viscous stress in the x-direction is $0{\cdot}17\ Nm^{-2}$. In the stably stratified flows presented below the basic density gradient, which the thermal boundary conditions are set to maintain, is such that the Brunt-Väisälä frequency, $N = \left(-\frac{g}{\rho}\frac{\partial \rho}{\partial z}\right)^{1/2} = 10^{-2}s^{-1}$.

The streamfunctions presented below are flows after 3000 time steps from the initial conditions. This is usually about sixty L/U_0 time scales and can be considered to be effectively an equilibrium state.

(a) Comparison with triple deck theory

To examine how the results of triple deck theory compare with those of the Navier-Stokes equation integrations it is desirable to see how the agreement depends on $\varepsilon = Re^{-\frac{1}{4}}$ which triple deck theory requires to be asymptotically small. This implies very large values of Reynold's number and the consequent breakdown of the flow into turbulence. For an Ekman boundary layer the first such Reynold's number dependent instability to occur is the so called class A viscous instabilities (see eg Lilly 1966) at $Re \approx 55$. At $Re \approx 125$ the class B or inflexion point instabilities with higher growth rate occur. The modes of maximum growth rate for these instabilities have an orientation at a small angle to the geostrophic flow direction. In the two dimensional flows presented here any instabilities are restricted to being at right angles to the geostrophic flow direction, and Ekman boundary layer instabilities are consequently stabilised. Without conducting an extensive survey, but by integrating our Navier-Stokes equation model with an initial perturbation, we have established that $Re \lesssim 600$ is stable while at $Re \gtrsim 1{,}000$ instabilities occur. This limits the value of ε to ~ 0.2. To obtain smaller ε we have exploited the fact that Ekman instabilities have slow growth rates and are sensitive to stabilisation with horizontal diffusion. In the following Navier-Stokes equation results we have chosen ν_H such that $R_H = \frac{U_0 L}{\nu_H} = 160$. This value gives negligible horizontal viscous stress gradients and thus leaves the basic

dynamics unchanged but stabilises the flow to instabilities with Re $\approx$ 2500 (ϵ = 0.14).

Fig 2 shows dimensionless stress and pressure from Navier-Stokes equation model neutral flows with ϵ = 0.2 and 0.14, together with results from triple deck theory. As is clear from the surface stress the flow possesses a small separation bubble. The other general features are as expected for this type of flow (Smith 1973) except for the absence of the downstream pressure maximum, due to the relatively short periodic domain. The main result of this comparison is that agreement is as good as could be expected for the values of ϵ used. The values of ϵ are not sufficiently spaced to demonstrate convergence to the triple deck results but the discernable trend is encouraging. A further comparison of total forces is made below in § 4(d).

(b) The effect of horizontal diffusion

Owing to the nonlinear cascade of energy to the smallest scales, if a non-physical build-up of energy on the smallest scales is to be prevented, there is a computational requirement for adequate viscous dissipation. The value of ν_0 we are using is typical of a vertical eddy diffusivity in the atmospheric boundary layer, and for integrations with horizontal topographic scales of the order of or less than the boundary layer depth, no non-physical amount of energy occurs on the smallest scales, using $\nu_H = \nu_0$. When the horizontal length scales are much greater than the boundary layer depth ν_H is required to be $>> \nu_0$ to effect closure. Suitable values of ν_H can be found empirically. Such values depend on the exact flow but we have found $R_H \approx 480$ to be typical in the present study. This is similar to the values appropriate to the

atmospheric boundary layer. Atmospheric values of ν_H can be derived from measurement of horizontal turbulent energy and spectral scales or more simply by observing that all components of the Reynolds stess tensor have roughly the same magnitude. When using an eddy viscosity parameterisation this implies

$$\nu_H \frac{\partial u}{\partial x} \sim \nu_0 \frac{\partial u}{\partial z}$$

$$\text{ie} \quad \nu_H \frac{U_0}{L} \sim \nu_0 \frac{U_0}{\delta}$$

$$\text{and} \quad R_H = \frac{U_0 L}{\nu_H} \sim \frac{U_0 \delta}{\nu_0} = Re$$

For the parameters considered in the present integrations Re = 630. We should emphasise that in most cases the effect of varying R_H around this typical value is found to be very small. In particular, steady flows with and without separation and strongly unsteady flows are not much affected. As might be expected, in the case of violent separation, the critical height of topography necessary for eddy shedding to occur is slightly increased by a reduction in R_H. However a more significant change in flow type with varying R_H occurs at particular parameters for which the separation bubble and wake appear to be subject to a weak instability; low values of R_H appear to be capable of completely suppressing this instability.

In producing fig 3 a-f we have chosen scales which we have found to favour this instability. The height of the hill (h = 300 m) is similar to the boundary layer depth and the length (L = 5 kms) gives a good sized separation bubble for small R_H. Fig 3 a and b show the steady separation bubbles at R_H = 80 and 160 respectively. The separation bubble for R_H = 80 is slightly smaller, but the close similarity of the flows confirms that ν_H is unimportant apart from suppressing the eddies. This unimportance was also confirmed in the previous section by the good agreement between triple deck solutions and Navier-Stokes integrations with large ν_H. Fig 3 c with R_H = 320 is similar but shows a weak unsteady downstream eddy. Fig 3 d and e with R_H = 640 and 1280 show larger unsteady eddies which become increasingly vigorous and extend further downstream as R_H is increased. Finally fig 3 f has $\nu_H = \nu_0$ giving $R_H = 10^4$, in this case the eddies persist all the way around the periodic domain. Some energy has built up to a steady value on grid scales though this is not obvious in the stream function.

Similar eddies with a wavelength of 2-3 kms occur for a small range of scales of topography whose height is comparable with boundary layer depth. This is the same wavelength as typifies the inflexion point instability occurring at larger unstable values of Re. As we mentioned in § 4 a the basic state for these integrations with Re = 630 is stable even with $\nu_H = \nu_0$, and the instabilities which occur at larger values of Re are easily suppressed with the use of larger ν_H. General energetic considerations make it clear that the separation bubble and wake, with flow reduced near the ground and accelerated higher up, may be susceptible to an instability of the inflexion point type. We are thus inclined to tentatively suggest that the instabilities are related to the inflexion point instability but defer a more detailed discussion to a future paper presenting the results of 3-dimensional numerical integrations of this type of flow.

(c) Flow characteristics

In this section we give an impression of the character of the various types of flow seen in the present study. We exclude the downstream eddies displayed in the previous section and concentrate on flows which are insensitive to R_H In all the examples present $R_H = 480$, a value which when used with the scales of fig 3 gives only a few weak downstream eddies.

(i) Homogeneous flows

To illustrate the range of flow types, we consider a fixed horizontal scale, L = 3 km, and presents results for variation of the height, h. Figures 4 a-d show the streamfunctions for h = 75, 150, 300, and 600 m respectively. When h = 75 m, the slope is small ($\sim$ 1/20), the flow is attached, and the streamlines are only slightly deflected by the topography. Increasing h to 150 m (slope $\sim$ 1/10) gives a steady separation bubble, rather smaller than the topography. The velocity components and pressure field for this particular flow are presented in figure 5. The horizontal velocity component, u, shows the reversed flow region in the lee of the ridge, and an increase in shear along the upper edge of the separation bubble. The velocity profile at the edge of the box is not very different from the undisturbed Ekman layer profile. The vertical velocity component, w, shows the localised influence of the ridge. The pressure field is precisely as expected in this relatively simple flow. There is a minimum in the surface

pressure just downstream of the summit, and a maximum at the leading edge of the hill. The pressure has a vertical scale similar to its horizontal scale. As explained in Mason and Sykes (1978a) pressure is actually defined under the ridge in the numerical model. Finally, the transverse velocity component, v, is hardly influenced by the presence of the ridge; the contours are simply displaced vertically by an amount roughly equal to $S(x)$. The profile at the edge of the domain is again very close to the undisturbed profile.

Returning to figure 4 c, increasing h to 300 m causes the flow to become unsteady. As h increases, the separation bubble becomes larger, and more unstable to shear instabilities. Figure 4 c shows an instantaneous picture of the streamfunction, which consists of large eddies which are shed from the back of the ridge, and roll downstream. These eddies are not sensitive to the value of R_H.

Increasing h to 600 m, figure 4 d, results in even larger eddies filling the domain. Instantaneous pictures of the other fields for this flow are presented in figure 6. The pressure field is completely dominated by the eddies, as is the vertical velocity field. The vertical extent of the disturbances is clearly much greater than the height of the topography. The flow is very chaotic, and resembles a deep "turbulent" boundary layer. This is evinced by the transverse velocity component, v, which shows a well-mixed region with strong gradients at the bottom. The v-field is almost a passive scalar field in these flows.

Detailed interpretation of the unsteady flows in figures 4 c and d is not useful, since a real flow would not remain two-dimensional in such chaotic conditions. Regular eddy-shedding is not achieved in these flows because of the periodicity. The separation bubble extends downstream fairly quickly as the height of the ridge increases, and soon interferes with the upstream flow. This appears to make the system more unstable; and when eddies are shed they travel around the domain, again directly affecting the incident flow.

An average shedding frequency, , can be calculated by examining the oscillations in the pressure force on the ridge. This gives a Strouhal number $\omega L/U_0 \sim 2$ for all the unsteady flows we have examined, including those in figure 4. However, there does seem to be a real difference in character between the eddies in figures 4 c and d, and those of the previous section. The eddies in figure 3 seem to be on a smaller length scale relative to the topography, and are a weak instability occurring only for special parameter values. The eddies in the present flows are much more violent, and not sensitive to the value of horizontal viscosity. It is possible that they are a manifestation of the same instability mechanism as those in figure 3, but under conditions when the instability is much stronger.

(ii) Stably stratified flows

In the homogeneous flows the topographic slope was the most important parameter but in stratified flows the horizontal length scale can be equally important. The relevant parameter is the Froude number $F_H = \frac{2\pi U_0}{NL}$, which measures the relative frequency of the motion $2\pi U_0/L$ to that of the stratification. For $F_H \gg 1$ ($L \ll$ 6 km here) the stratification has little effect, but for $F_H \lesssim 1$ waves will be excited. When h is large enough to give $U_0/Nh \lesssim 1$ separation in the lee of the hill is suppressed as dense fluid lifted over the summit falls rapidly to its equilibrium level. Otherwise separation is inhibited when the wavelength of gravity waves coincides with the scale of the topography. Upstream separation where fluid near to ground level cannot be lifted over the summit may also occur. In fig 4 e-g the stratified counterparts to fig 4 a-d are presented. On this horizontal scale the shortest possible gravity wave has wavelength 6 kms and corresponds to $\sim$ 2 wavelength in the periodic domain. With h = 75 m a slight wave is evident and less stress reduction in the lee of the hill is seen. When h = 150 m separation has been suppressed and the wave generated is seen to give a stress reduction at the edge of box. In this and the other results presented the wave energy appearing downstream has not been reflected off the lid, where a radiation condition is simulated, but has propagated horizontally. For h = 300 m steady upstream and downstream separation occurs and the wave amplitude is sufficient to

give a steady rotor. Finally with h = 600 m the flow has become unsteady but the eddy intensity and height are somewhat reduced from the homogeneous case.

The downstream eddies illustrated in fig 3 a-c have not been found in any stratified flows. This is consistent with suppression of inflexion point instabilities by stable stratification (Kaylor and Faller 1972).

(d) Net forces

In Tables 1 and 3 we give the changes in net forces over a range of height and length scales for homogeneous and stratified flows respectively. F_T is the sum of the pressure and the total viscous forces on the surface $z = S(x)$ in the U_o direction and F_o is the component of the total undisturbed viscous force in the U_o direction (ie the force in the absence of topography). The angle α is defined as $\tan^{-1} F_y/F_T$, where F_y is the total viscous force in the y-direction. The character of the flow and the relative size of the pressure force F_p are also indicated. The forces presented are the final, or for unsteady flows a time average, occurring after integrating for a time of about $60\, L/U_o$. After this time the flows are not completely steady as unimportant changes are inevitably still occurring on a time scale ζ^{-1}. As a result of this unsteadiness we estimate changes in total force $F_T - F_o$ to have a typical accuracy of 10%.

(i) Homogeneous flows

At high Reynolds numbers, the pressure force on the hill would be expected to be of order $\bar{\rho}\,\bar{U}^2 h$, where $\bar{U}$ is some average velocity incident on the ridge and $\bar{\rho}$ is the mean density, taken to be unity. Thus for a constant shear flow, it follows that the pressure force could increase as rapidly as h^3. In the present results, this rate of increase is limited by the finite boundary layer depth, and also by changes in the incident velocity profile due to the periodicity of the domain. Table 1 shows a rapid initial increase in pressure force with h, tailing off when the ridge is sufficiently high for its wake to fill the domain. On the other hand, the total force on the surface, and its direction, hardly changes from the undisturbed value during the initial increase in h.

The total force rises dramatically when the flow becomes unsteady.

For steady flows, even when separation occurs, the pressure force is almost completely balanced by a reduction in viscous force. This near zero increase in net drag in spite of large pressure forces on the topography is exactly what is predicted by triple deck theory for small ϵ. For finite ϵ a second-order steady linearised analysis by Brighton (1978) gives a force depending on h^2. Results for the present cases are given in Table 2 and can be seen to be of the observed magnitude for steady flows. Better agreement cannot be expected since none of the flows are linear. Any apparent agreement in the unsteady regime is fortuitous.

In the unsteady flows, the large eddies tranfer momentum vertically, increasing the viscous surface stress in both the x- and y-directions. The actual value of the resultant viscous stress is strongly affected by the periodic boundary conditions. For the most violent flows presented here, the average viscous stress in the x-direction is almost zero, and the total force is entirely due to the pressure force. As noted in the previous section, for these violent flows the pressure field is dominated by the large eddies, and the instantaneous pressure force may change sign.

Table 1 also serves to illustrate how, whilst the occurrance of separation depends primarily on topographic slope, larger values of h give separation more easily than smaller ones of the same slope. This is because the larger values of h correspond to larger vertical Reynolds numbers, $U_o h / \nu_o$

(ii) Stably stratified flows

As is particularly evident on the larger horizontal scales, for these cases gravity wave radiation can give a contribution to the total force F_T. Separation and eddies are seen to be inhibited except for the $h = 600$ m cases in which upstream separation occurs even with $L = 3.10^4 m$. To judge the results we can compare with inviscid linear theory (Queney 1947) and triple deck equation solutions (Sykes 1978). Results are given in Tables 4 and 5 respectively. For $L = 10^3 m$ the domain is too short to

support gravity waves and no radiation can occur. As a consequence of eddy suppression the total forces are reduced in comparison with the homogeneous flows. For other values of L gravity wave radiation occurs and when eddies are absent the drag increase is primarily due to this. The linear theory, as would be expected with its supposition of the vertical velocity on $z = S(x)$ being $U_0 \frac{dS}{dx}$, overestimates the drag by a factor of between 2 to 4, being most inaccurate for small h and L. The triple deck solutions include the viscous boundary layer and agreement is generally better, especially for the smaller hills.

5. Conclusions

Over a wide range of scales relevant to the atmosphere we have shown that homogeneous laminar unseparated and steady separated flows give no net increase in the total force acting on the lower boundary. This result is predicted by triple deck theory for small values of the parameter ϵ and its validity for larger values of ϵ is confirmed by the good overall agreement between triple deck solutions and Navier-Stokes equation integrations. The integrations also show that the generation of large eddies by the topography is the main mechanism giving an increase in total drag. These are found to occur with violently separated flows. An exception to this generation mechanism is what appeared to be a downstream instability and which we tentatively suggest is related to Ekman layer inflexion point instability. These instabilities behave quite differently in three-dimensional flow when they can take an energetically more favourable orientation to the mean flow (Mason and Sykes 1978c). Likewise, no significance can be placed on the exact values of results for violent separation, due to the imposition of two-dimensionality.

In the stably stratified flows the Navier-Stokes equation integrations showed how on many scales a total drag reduction, through eddy suppression, occurred even though gravity wave radiation was also taking place. With regard to the value of gravity wave drag in less violent flows the integrations confirmed the triple deck theory results (Sykes 1978) which showed that the inviscid theory overestimated gravity wave drag.

Overall we have identified a number of important features of the effect of topography on laminar flow on atmospheric scales. These features have potentially important implications for the parameterisation of topography in numerical models and it is an urgent matter to extend this work to include turbulence modelling of a standard able to give useful results with mean flows of the type seen here. This forms part of our current research programme. For the present we feel able to speculate that the basic nature of the results may not be altered. This is based on our feeling that the main effects arise from mean flow eddies and preliminary results from a crude eddy viscosity turbulence model with "log layer" boundary conditions and valid for small topographic slope.

Table 1. Total forces and flow character in homogeneous Navier-Stokes integrations: S - denotes steady separation and E - denotes eddy shedding.

h \ L	10^3 m	3×10^3 m	10^4 m	3×10^4 m
	$\frac{F_T}{F_o}$ ∝ $\frac{F_p}{F_o}$	$\frac{F_T}{F_o}$ ∝ $\frac{F_p}{F_o}$	$\frac{F_T}{F_o}$ ∝ $\frac{F_p}{F_o}$	$\frac{F_T}{F_o}$ ∝ $\frac{F_p}{F_o}$
75 m	S 1.05 44 0.24	1.00 45 0.05	1.00 45 0.01	1.00 45 0.00
150 m	E 1.52 38 1.24	S 1.02 46 0.25	1.01 45 0.03	1.00 45 0.00
300 m	E 3.00 24 3.18	E 1.56 37 1.22	S 1.05 46 0.18	1.00 45 0.01
600 m	E 2.38 29 2.54	E 3.15 25 3.12	E 1.35 39 0.67	1.02 41 0.05

Table 2. Total force F_T/F_o from second order, linearised, triple deck analysis (calculated using ε = 0.2, etc).

h \ L	10^3 m	3×10^3 m	10^4 m	3×10^4 m
75 m	1.02	1.01	1.00	1.00
150 m	1.09	1.04	1.01	1.00
300 m	1.37	1.17	1.03	1.00
600 m	2.48	1.67	1.14	1.01

Table 3. Total forces and flow character in stratified Navier-Stokes integrations: S- denotes steady separation and E - denotes eddy shedding.

h \ L	10^3 m	3×10^3 m	10^4 m	3×10^4 m
	$\frac{F_T}{F_o}$ ∝ $\frac{F_p}{F_o}$	$\frac{F_T}{F_o}$ ∝ $\frac{F_p}{F_o}$	$\frac{F_T}{F_o}$ ∝ $\frac{F_p}{F_o}$	$\frac{F_T}{F_o}$ ∝ $\frac{F_p}{F_o}$
75 m	S 1.04 44 0.21	1.00 45 0.05	1.02 44 0.04	1.01 45 0.02
150 m	S 1.09 47 0.95	1.08 44 0.25	1.12 43 0.18	1.05 44 0.03
300 m	E 1.33 46 1.21	S 1.38 42 1.20	1.57 36 0.79	1.23 40 0.33
600 m	E 2.15 41 1.90	E 3.24 28 3.00	S 2.84 26 2.41	S 2.14 32 1.42

Table 4. Normalised wave drag, F_w/F_o. F_w is the inviscid wave drag calculated from linear theory.

h \ L	10^3 m	3×10^3 m	10^4 m	3×10^4 m
75 m	0	0.05	0.08	0.03
150 m	0	0.18	0.33	0.13
300 m	0	0.73	1.32	0.50
600 m	0	2.92	5.28	2.00

Table 5. Total force F_T/F_o from numerical stratified triple deck.

h \ L	10^3 m	3×10^3 m	10^4 m	3×10^4 m
75 m	1.00	1.01	1.02	1.01
150 m	1.00	1.06	1.10	1.04
300 m	1.00	1.28	1.46	1.19
600 m	1.00	1.50	2.50	1.82

Legends

Figure 1.

Illustrating the domain of the Navier Stokes equation integrations.

Figure 2.

Comparison between triple deck and Navier-Stokes results. (a) dimensionless surface stress $\tau^* = \frac{\delta}{u_0}\frac{\partial u}{\partial z}\Big|_{z=S(x)}$ and (b) dimensionless surface pressure $p^* = p/\epsilon^2 u_0^2$. The solid line denotes the triple deck solution and the crosses and circles the results of Navier-Stokes equation integrations with $\epsilon = 0.2$ and 0.14 respectively. The dimensionless value of the height of the topography $h/\epsilon\delta = 1.7$ and the dimensionless base width $\epsilon L/\delta = 1.11$.

Figure 3

Illustrating the effect of varying horizontal diffusion. (a) to (f) show streamfunctions obtained from the Navier-Stokes equations on a mesh of 64 x 40 points. $h = 300$ m and $L = 5.0\ 10^3$m. The values of R_H used are (a) 80 ; (b) 160; (c) 320; (d) 640; (e) 1280; (f) 10^4.

Figure 4.

Illustrating the effect of varying height scale. (a) to (h) show streamfunctions obtained from the Navier-Stokes equations on a mesh of 64 x 40 points. In all cases $L = 3$ km and $R_H = 480$. Cases (a) to (d) are homogeneous and (e) to (h) stably stratified with $N = 10^{-2}s^{-1}$. The heights of topography, h, used are (a) and (e) 75 m; (b) and (f) 150 m; (c) and (g) 300 m; (d) and (h) 600 m.

Figure 5.

Velocity components and pressure for the flow illustrated in figure 4(b). (a) u-component of velocity, contour interval 1 ms^{-1}. (b) Pressure field, contour interval 0.5 Nm^{-2}. (c) v-component of velocity, contour interval 0.34 ms^{-1}. (d) w-component of velocity, contour interval 0.04 ms^{-1}. Solid lines denote positive contour values, negative values are, dashed. Note that contours are generated by linear interpolation between grid-points, and are consequently inaccurate close to the surface.

Figure 6.

Velocity components and pressure for the flow illustrated in figure 4(d). (a) u-component of velocity, contour interval 1 ms^{-1}, (b) Pressure field, contour interval 1.8 Nm^{-2} (c) v-component of velocity, contour interval 0.53 ms^{-1}. (d) w-component of velocity, contour interval 0.19 ms^{-1}.

References

Brighton, P W M (1978): 'Ekman layer flow over gentle two-dimensional obstacles'. submitted to J Fluid Mech.

Brown, S N & Stewartson, K (1969): 'Laminar separation.' A Rev Fluid Mech 1 pp 45-72

Browing, K A & Bryant, G W (1975): 'An example of rainbands associated with stationary longitudinal circulations in the planetary boundary layer.' Q J Roy Met Soc 101 pp 893-900.

Faller, A J & Kaylor, R E (1966): 'A numerical study of the instability of the laminar Ekman boundary layer'. J Atmos Sci 23 pp 466-480.

Hunt, J C R (1971): 'A theory for the laminar wake of a two-dimensional body in a boundary layer.' J Fluid Mech 49 pp 159-178.

Jackson, P S & Hunt, J C R (1975): 'Turbulent wind flow over a low hill.' Q J Roy Met Soc 101 pp 929-956.

Kaylor, R E & Faller, A J (1972): 'Instability of the stratified Ekman boundary layer and the generation of internal waves.' J Atmos Sci 29 pp 497-509.

Lilly, D K (1966): 'On the instability of Ekman boundary flow.' J Atmos Sci 23 pp 481-494.

Mason, P J & Sykes, R I (1978a): 'A simple Cartesian model of boundary layer flow over topography.' To appear in J Comp Phys.

Mason, P J & Sykes, R I (1978b): 'On the interaction of topography and Ekman boundary layer pumping in a stratified atmosphere.' Q.J.Roy.Met.Soc. 104 pp 475-490

Mason, P J & Sykes, R I (1978c): 'On the net forces produced by surface-mounted obstacles.' Submitted to Q.J.Roy.Met.Soc.

Messiter, A F (1970): 'Boundary layer flow near the trailing edge of a flat plate'. S I A M J Appl Math 18 pp 241-257.

Piacsek, S A & Williams, G P (1970): 'Conservation properties of convection difference schemes.' J Comp Phys 6 pp 392-405.

Queney, P (1947): 'The problem of airflow over mountains: a summary of theoretical studies.' Bull Am Meteor Soc 29 pp 16-27.

Smith, F T (1973): 'Laminar flow over a small hump on a flat plate.' J Fluid Mech 57 pp 803-824.

Smith, F T (1977): 'The laminar separation of an incompressible fluid streaming past a smooth surface.' Proc Roy Soc A356 pp 443-463.

Stewartson, K (1969): 'On the flow near the trailing edge of a flat plate.' Mathematika 16 pp 106-121.

Stewartson, K (1974): 'Multistructured boundary layers on flat plates and related bodies.' Adv Appl Mech 14 pp 145-239.

Sykes, R I (1978): 'Stratification effects in boundary layer flow over hills Proc.Roy.Soc. A361 pp 225-243.

Taylor, P A (1977): 'Numerical studies of neutrally stratified planetary boundary layer flow above gentle topography. I two-dimensional cases.' Boundary layer Met. 12 pp 37-60.

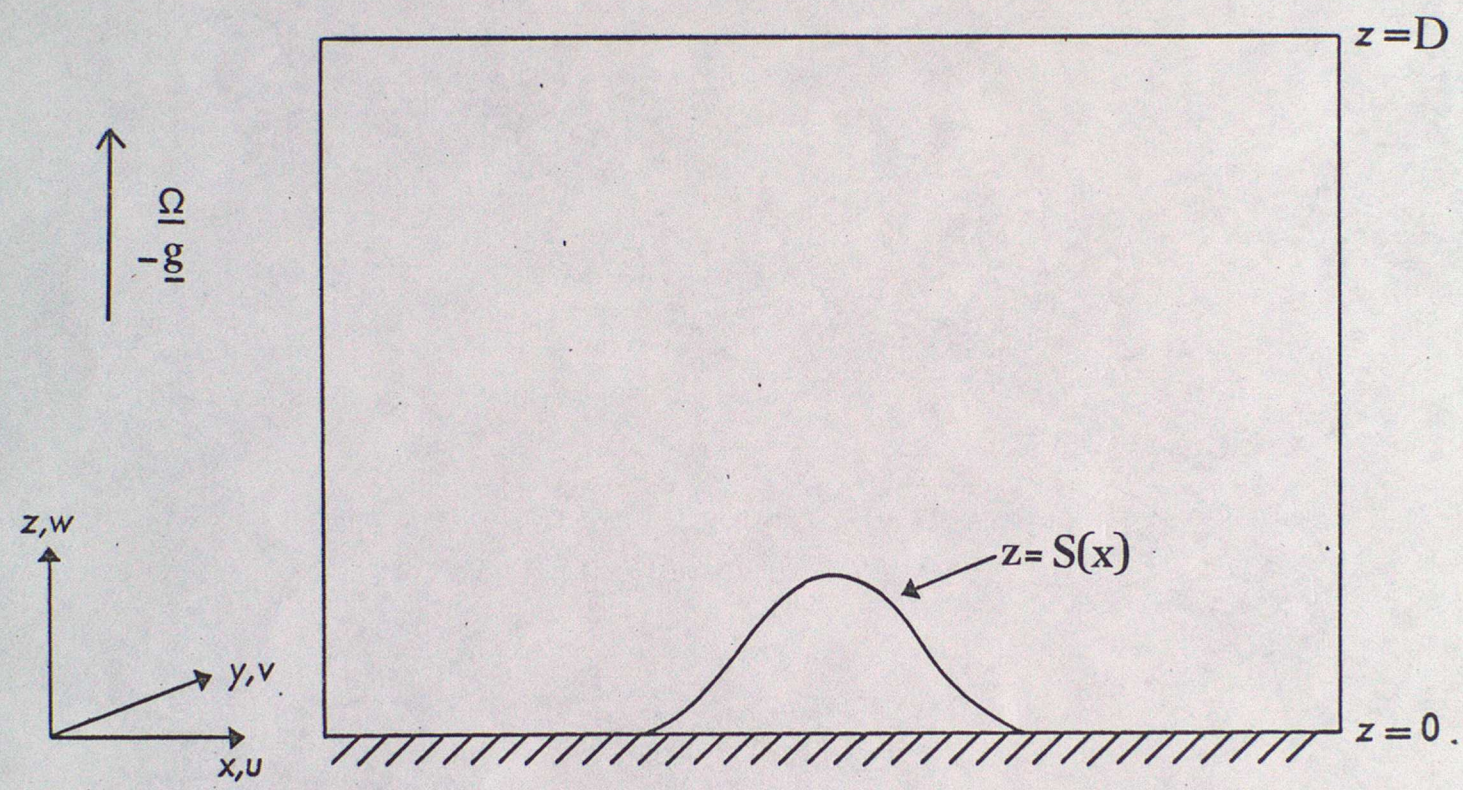

Figure 1

Fig 2a

Fig 2 b

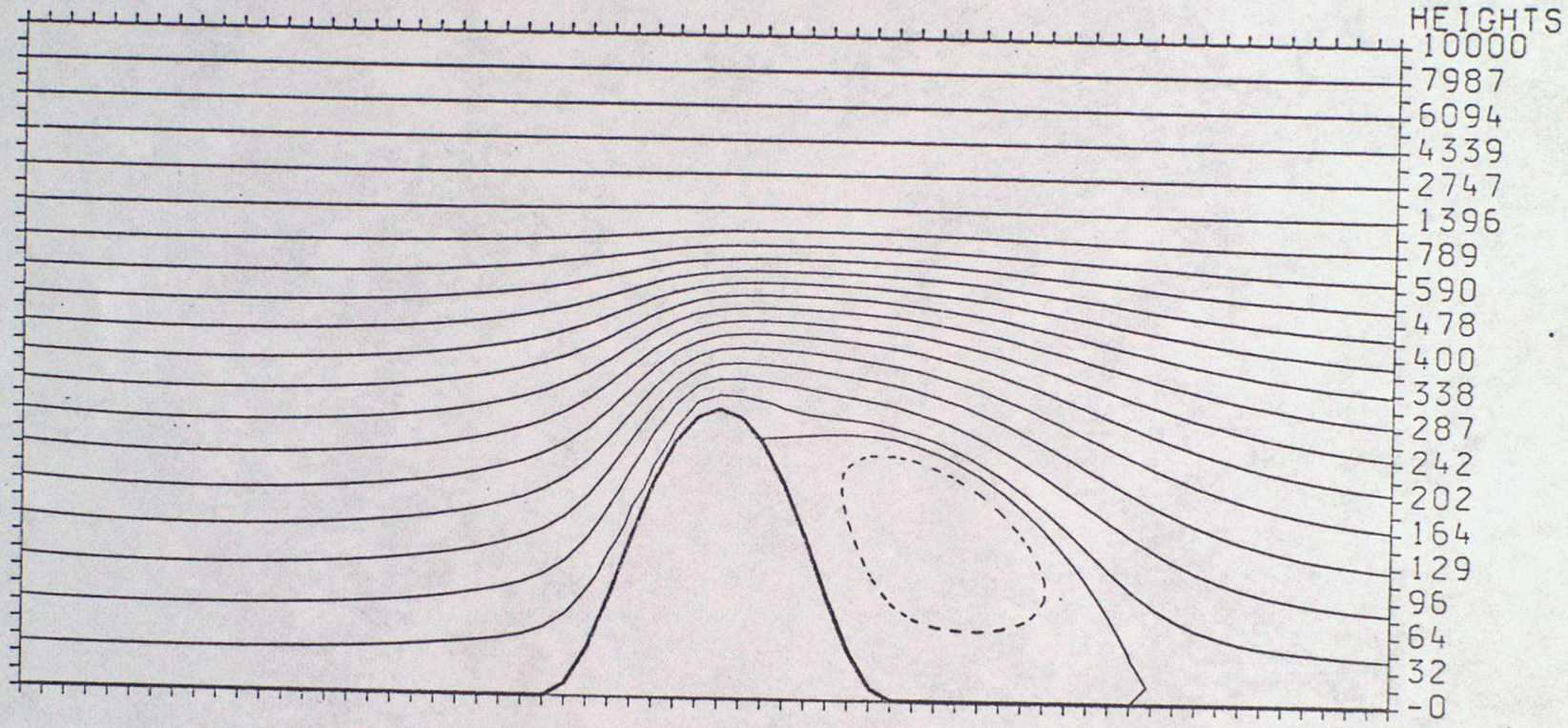
HEIGHTS
10000
7987
6094
4339
2747
1396
789
590
478
400
338
287
242
202
164
129
96
64
32
-0

Fig 3a

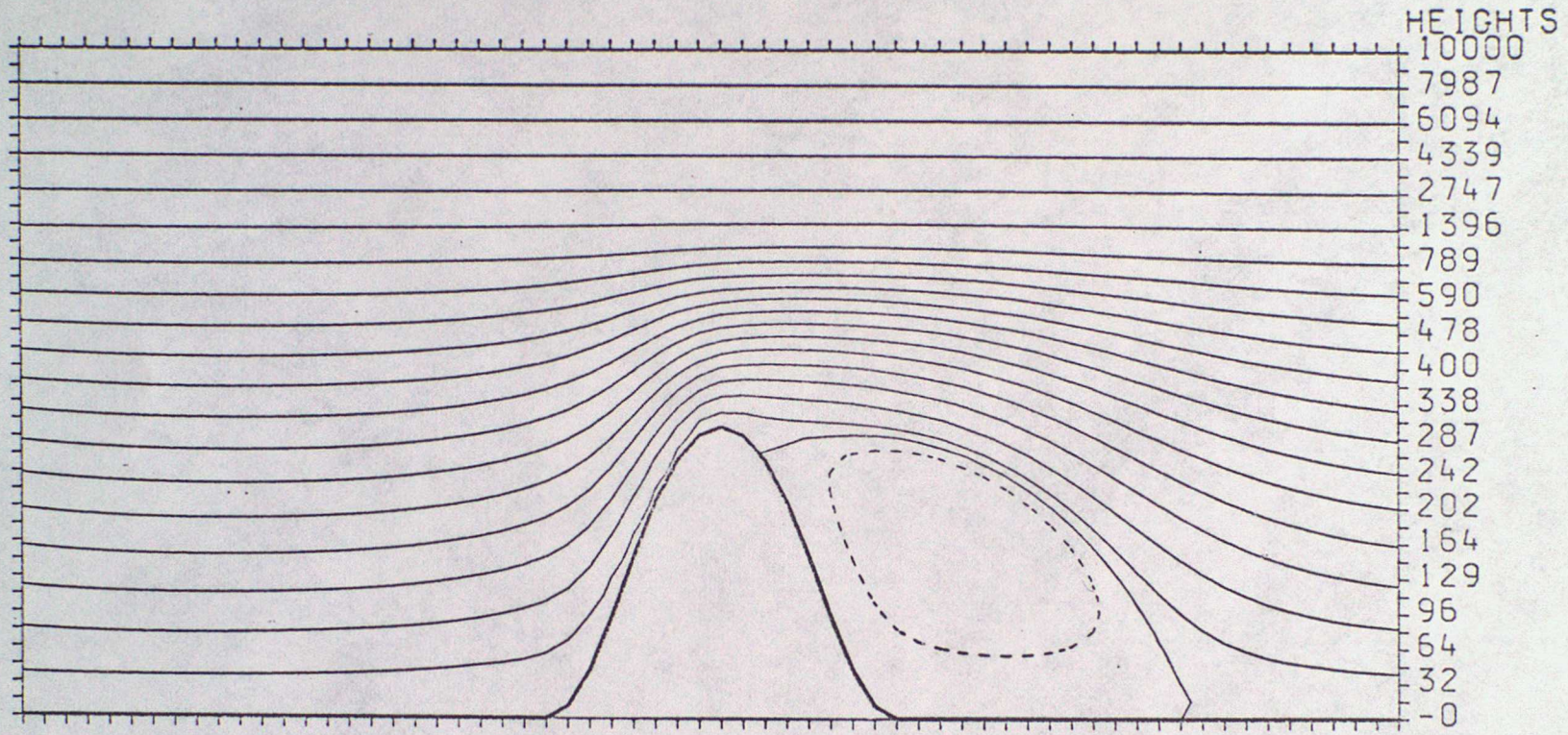
HEIGHTS
10000
7987
6094
4339
2747
1396
789
590
478
400
338
287
242
202
164
129
96
64
32
-0

Fig 3b

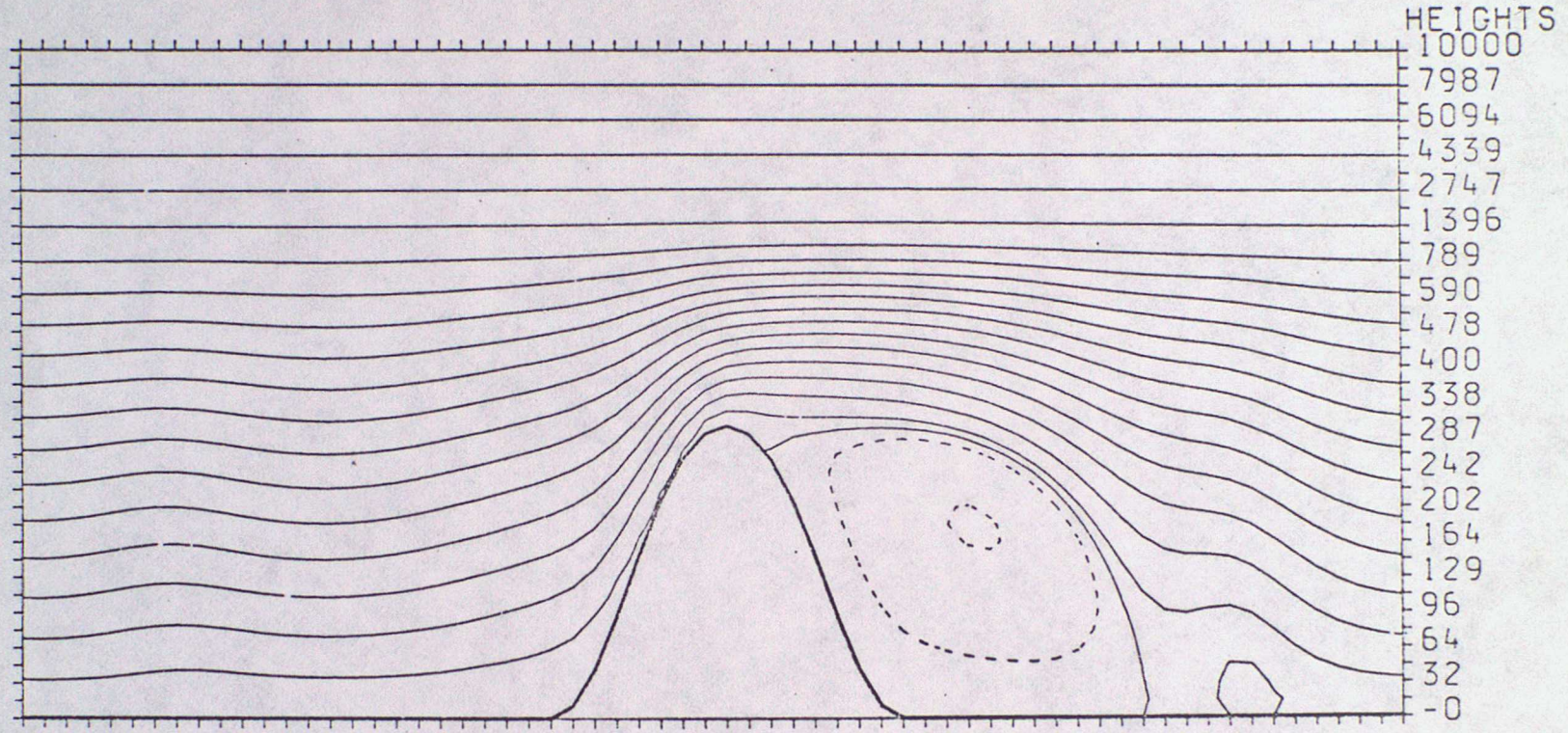
HEIGHTS
10000
7987
6094
4339
2747
1396
789
590
478
400
338
287
242
202
164
129
96
64
32
-0

Fig 3c

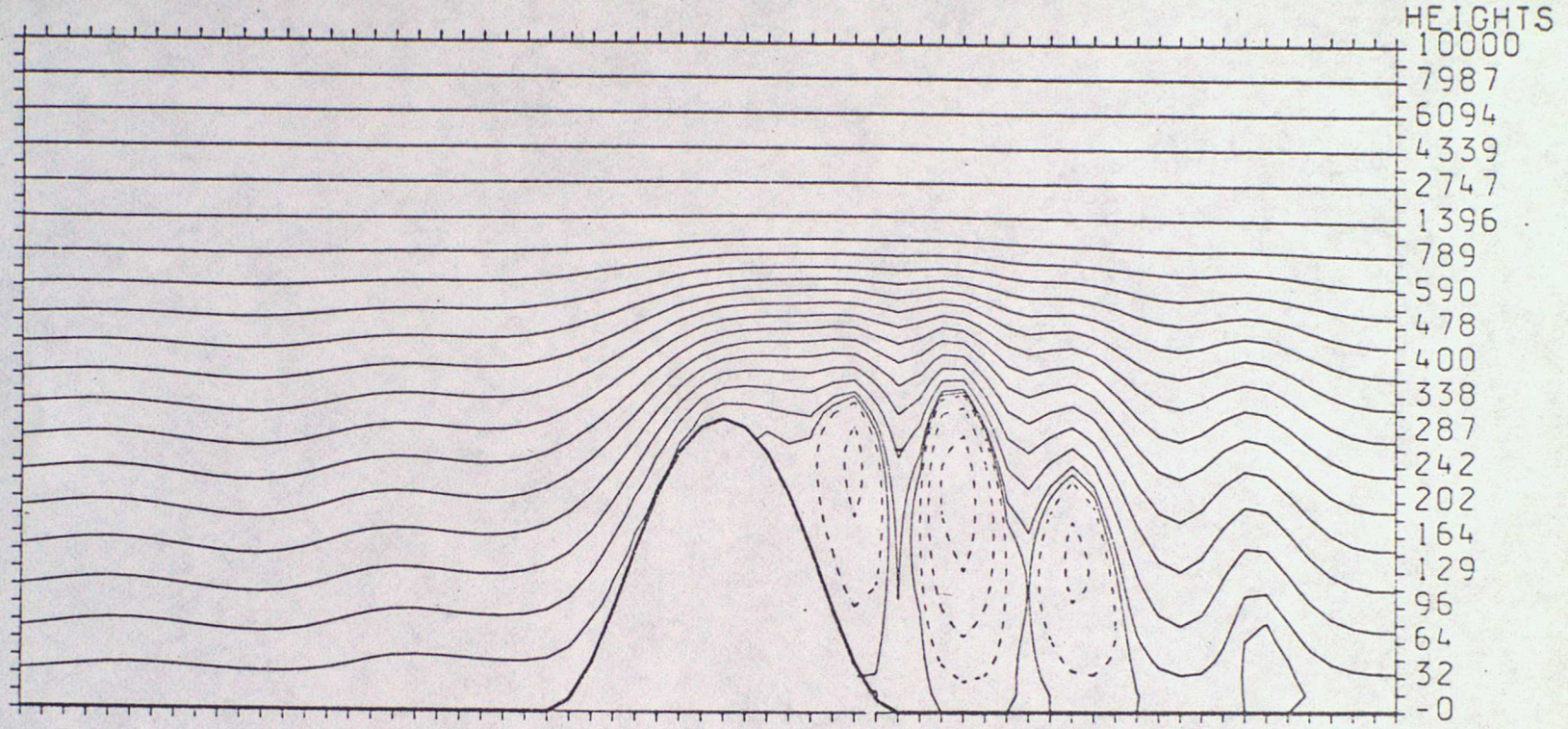
HEIGHTS
10000
7987
6094
4339
2747
1396
789
590
478
400
338
287
242
202
164
129
96
64
32
-0

Fig 8d

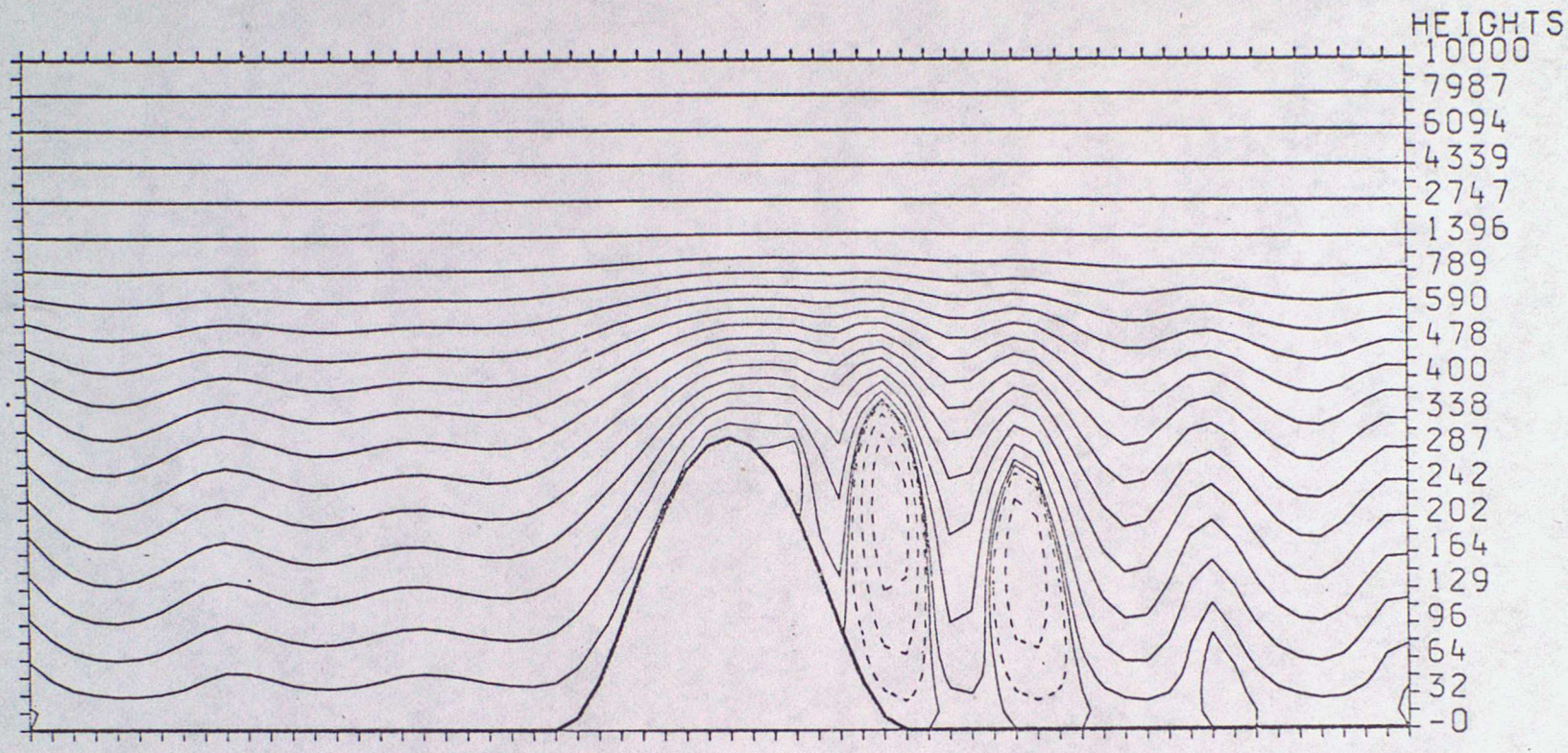
HEIGHTS
10000
7987
6094
4339
2747
1396
789
590
478
400
338
287
242
202
164
129
96
64
32
-0

Fig 3e

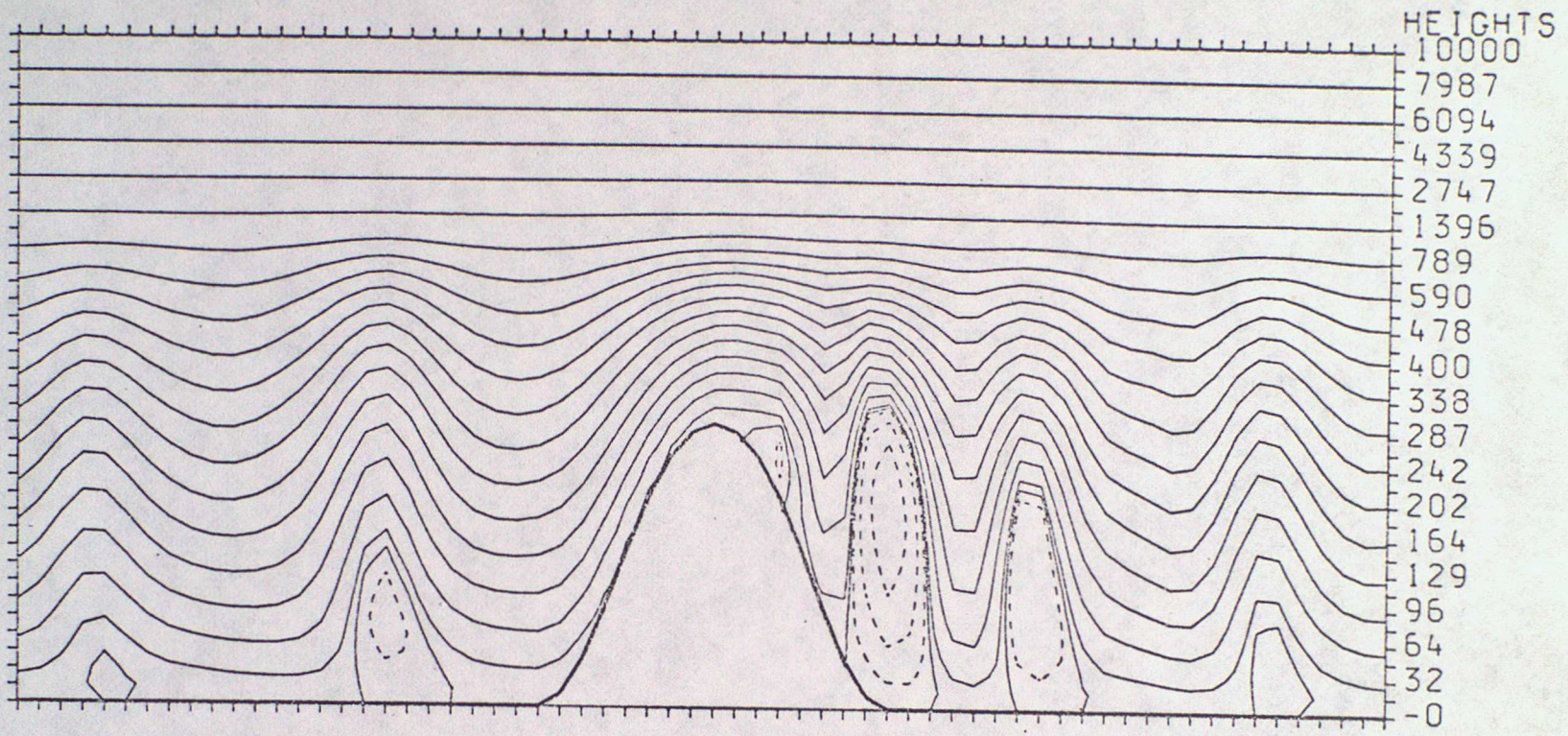
HEIGHTS
10000
7987
6094
4339
2747
1396
789
590
478
400
338
287
242
202
164
129
96
64
32
-0

Fig 3f

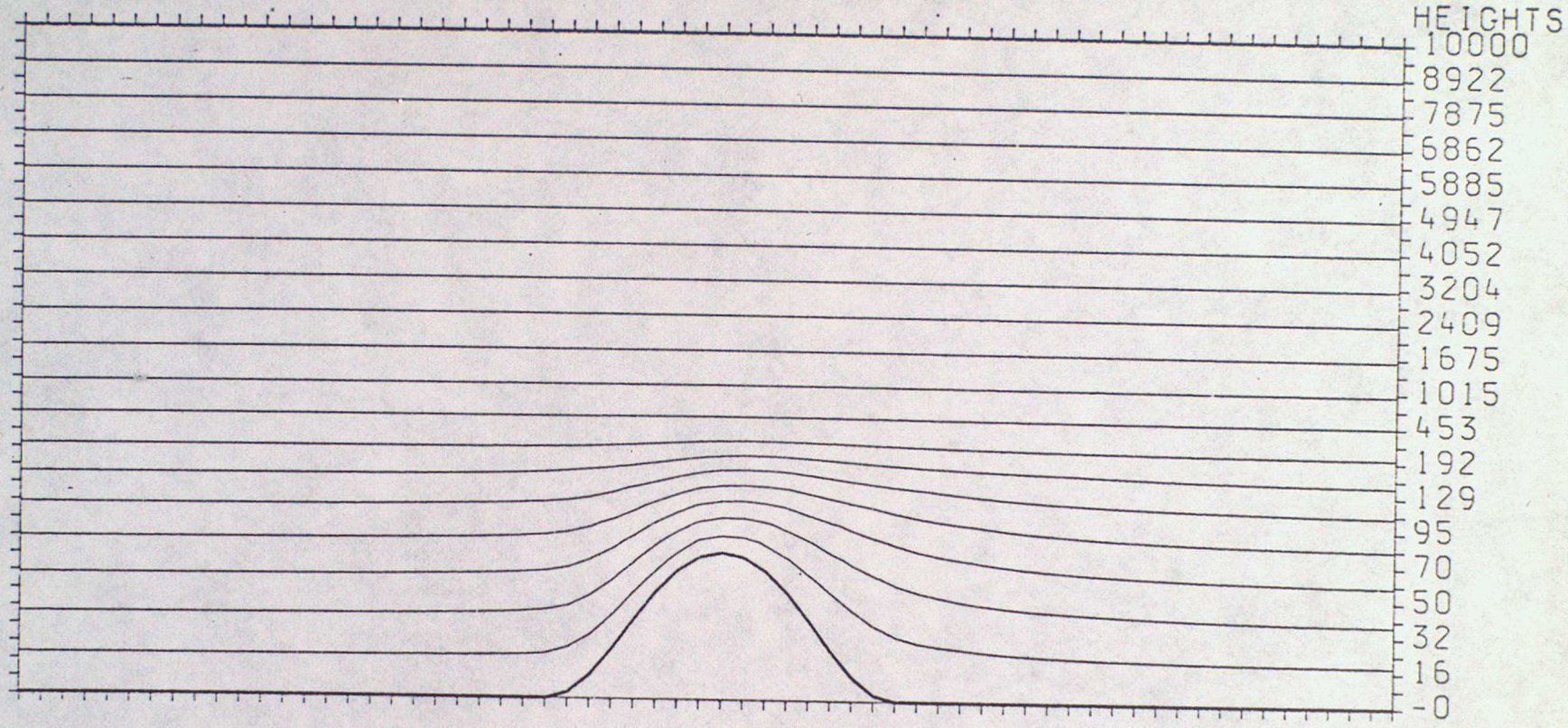
HEIGHTS
10000
8922
7875
6862
5885
4947
4052
3204
2409
1675
1015
453
192
129
95
70
50
32
16
-0

Fig 6.4a

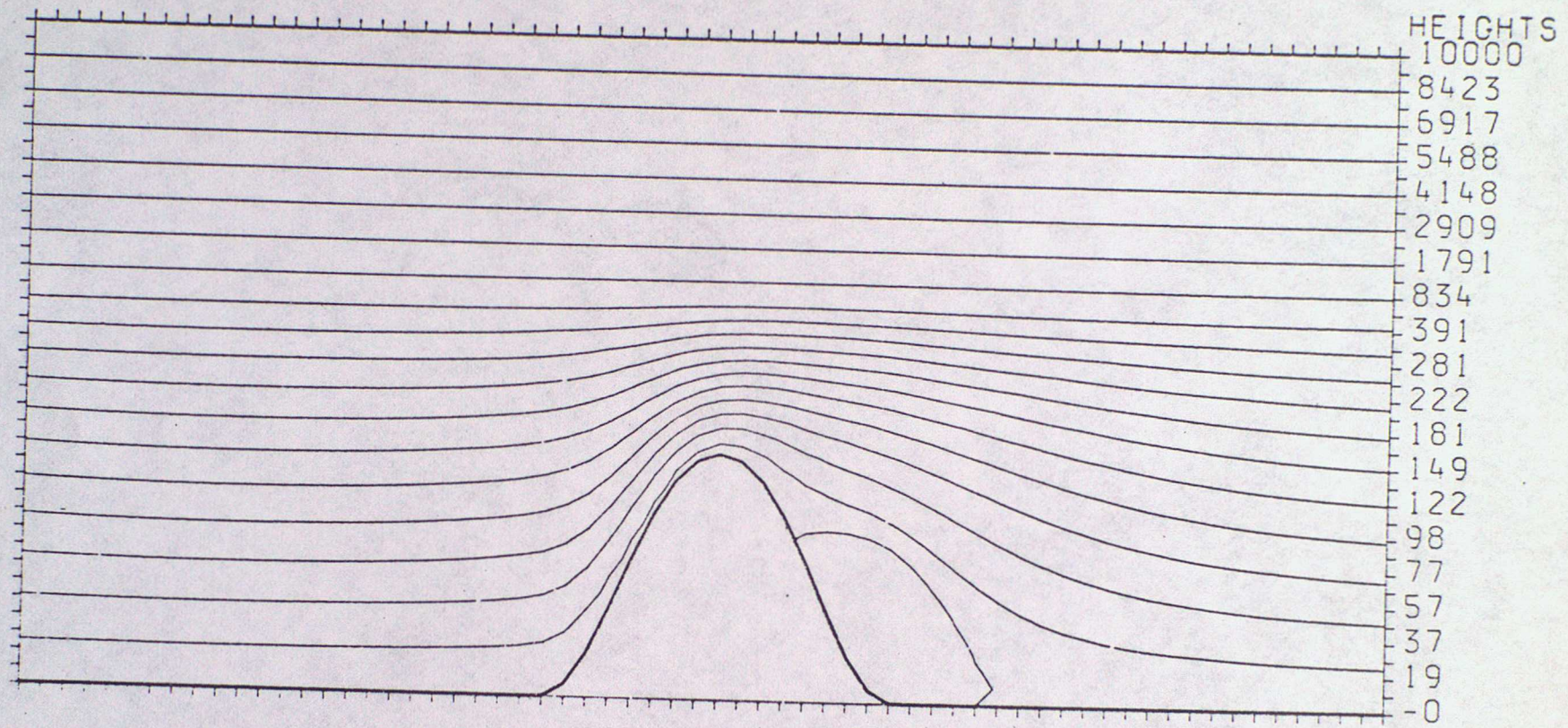
HEIGHTS
10000
8423
6917
5488
4148
2909
1791
834
391
281
222
181
149
122
98
77
57
37
19
-0

Fig 4b

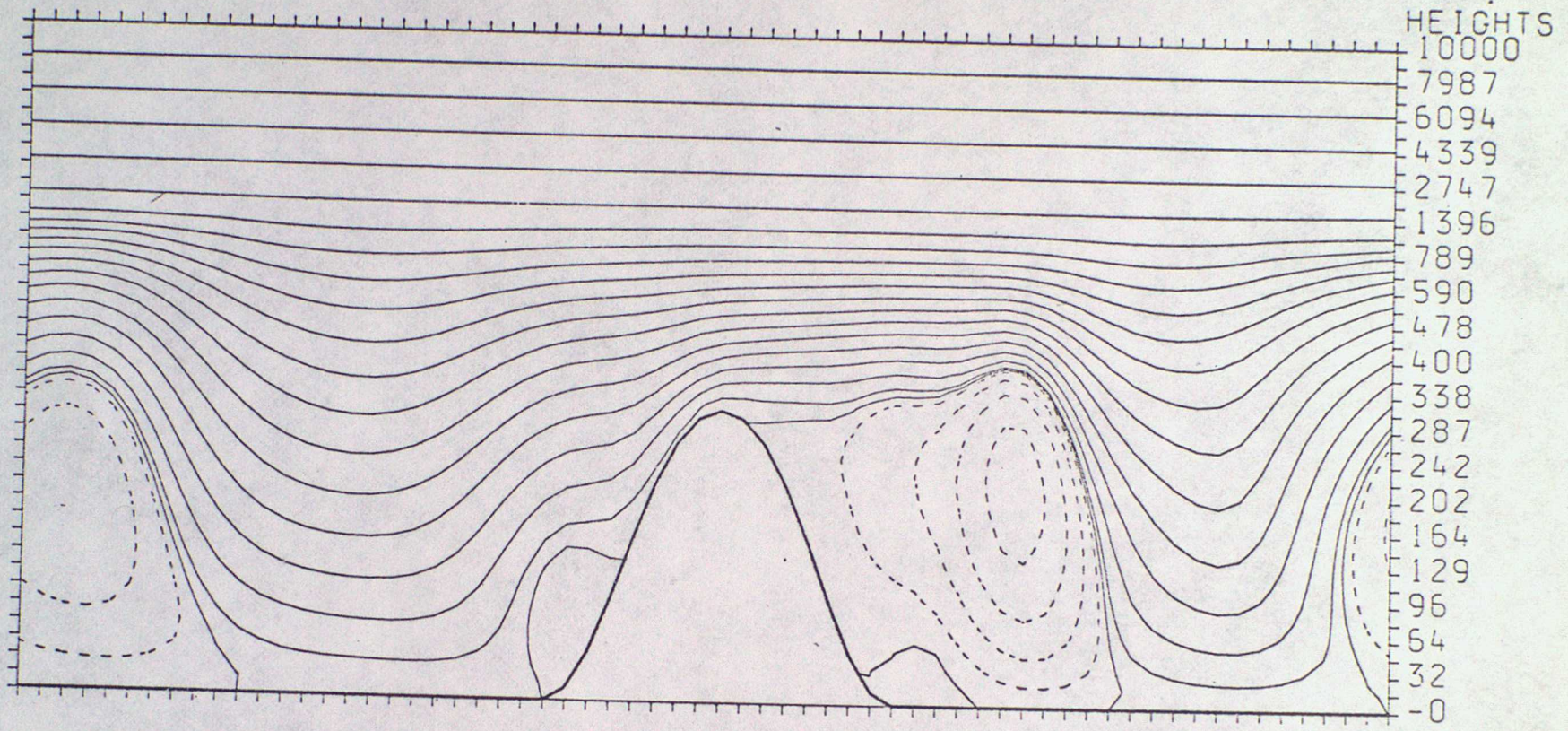
HEIGHTS
10000
7987
6094
4339
2747
1396
789
590
478
400
338
287
242
202
164
129
96
64
32
-0

Fig 4C

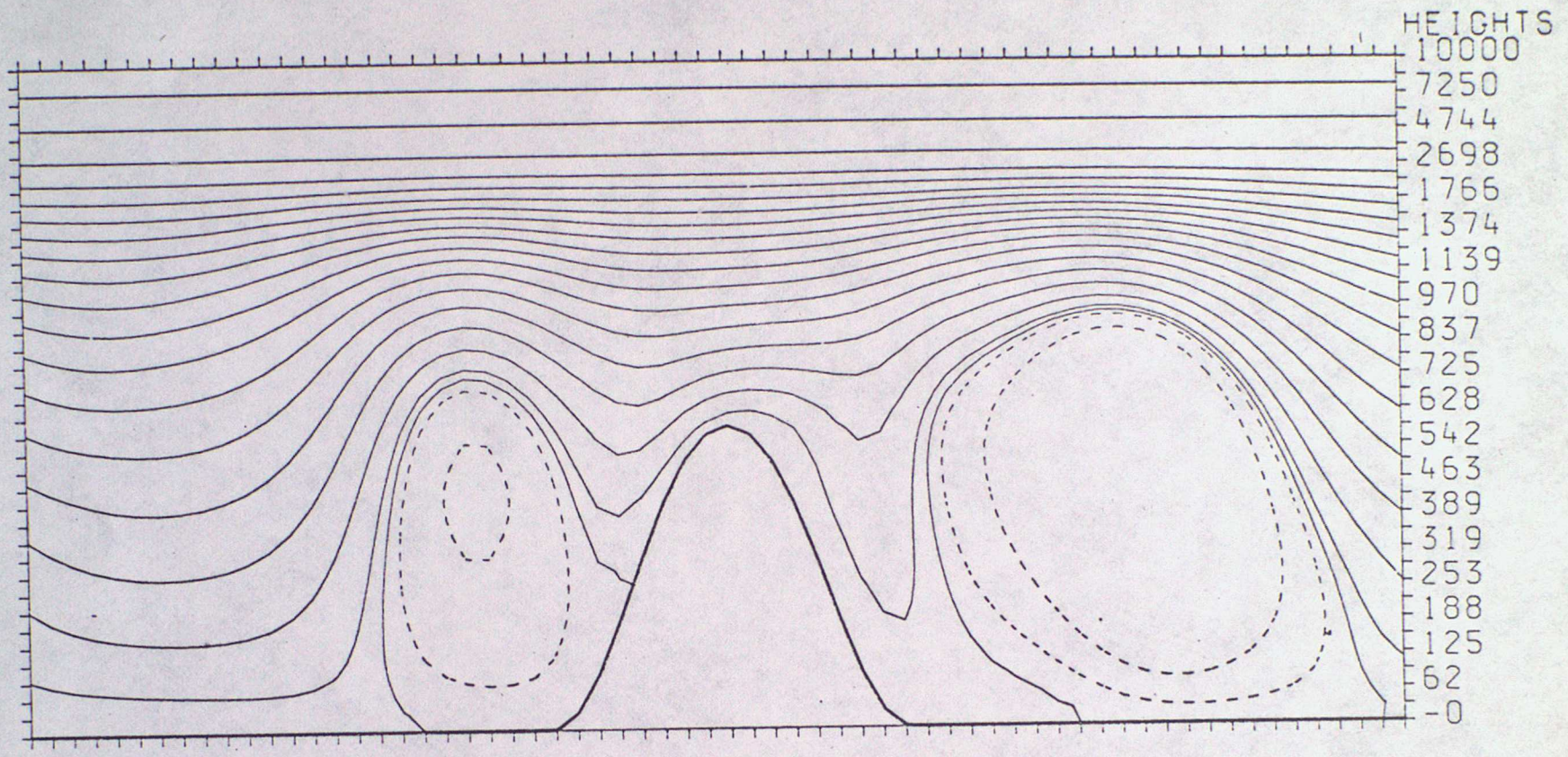
HEIGHTS
10000
7250
4744
2698
1766
1374
1139
970
837
725
628
542
463
389
319
253
188
125
62
-0

Fig 4d

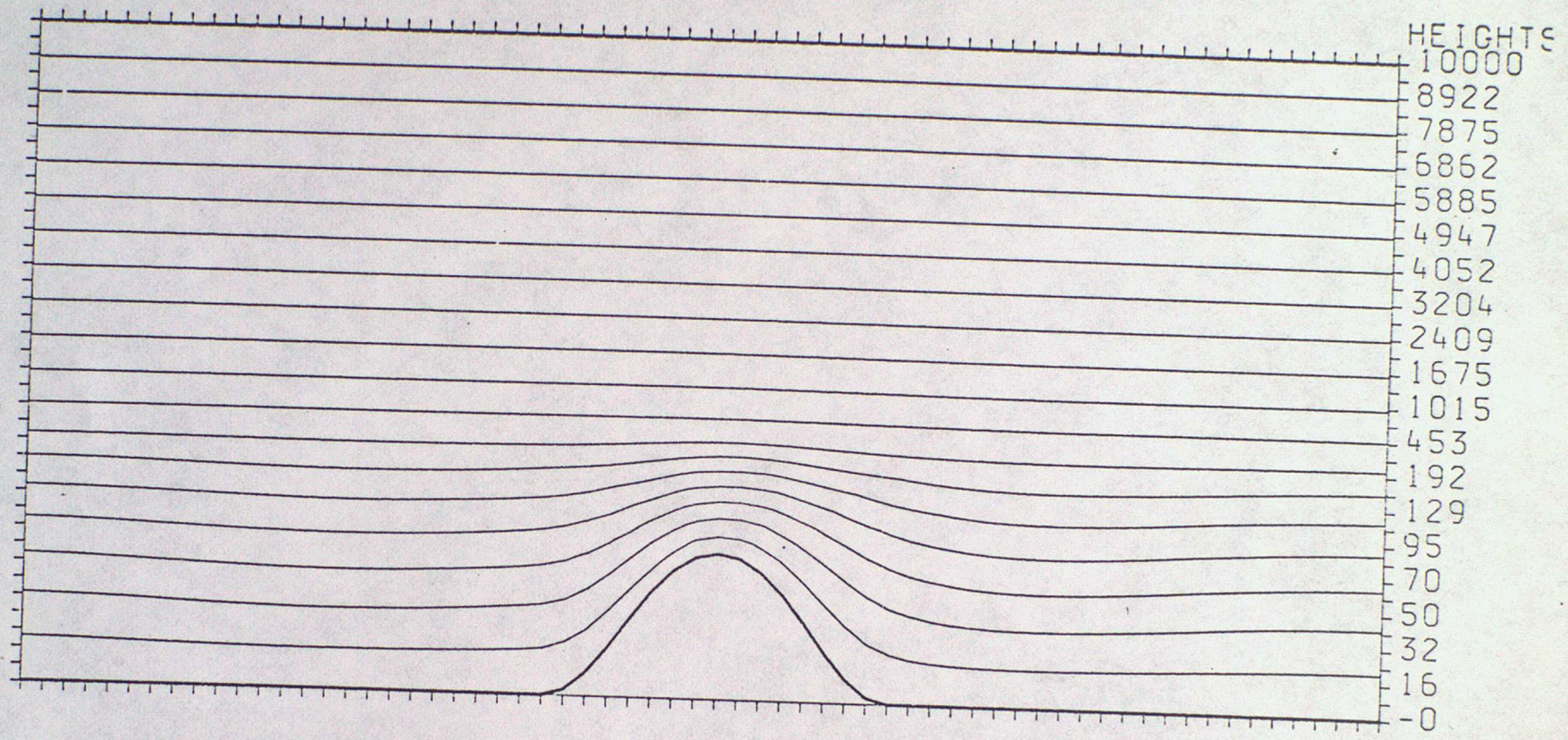
HEIGHTS
10000
8922
7875
6862
5885
4947
4052
3204
2409
1675
1015
453
192
129
95
70
50
32
16
-0

Fig 04e/

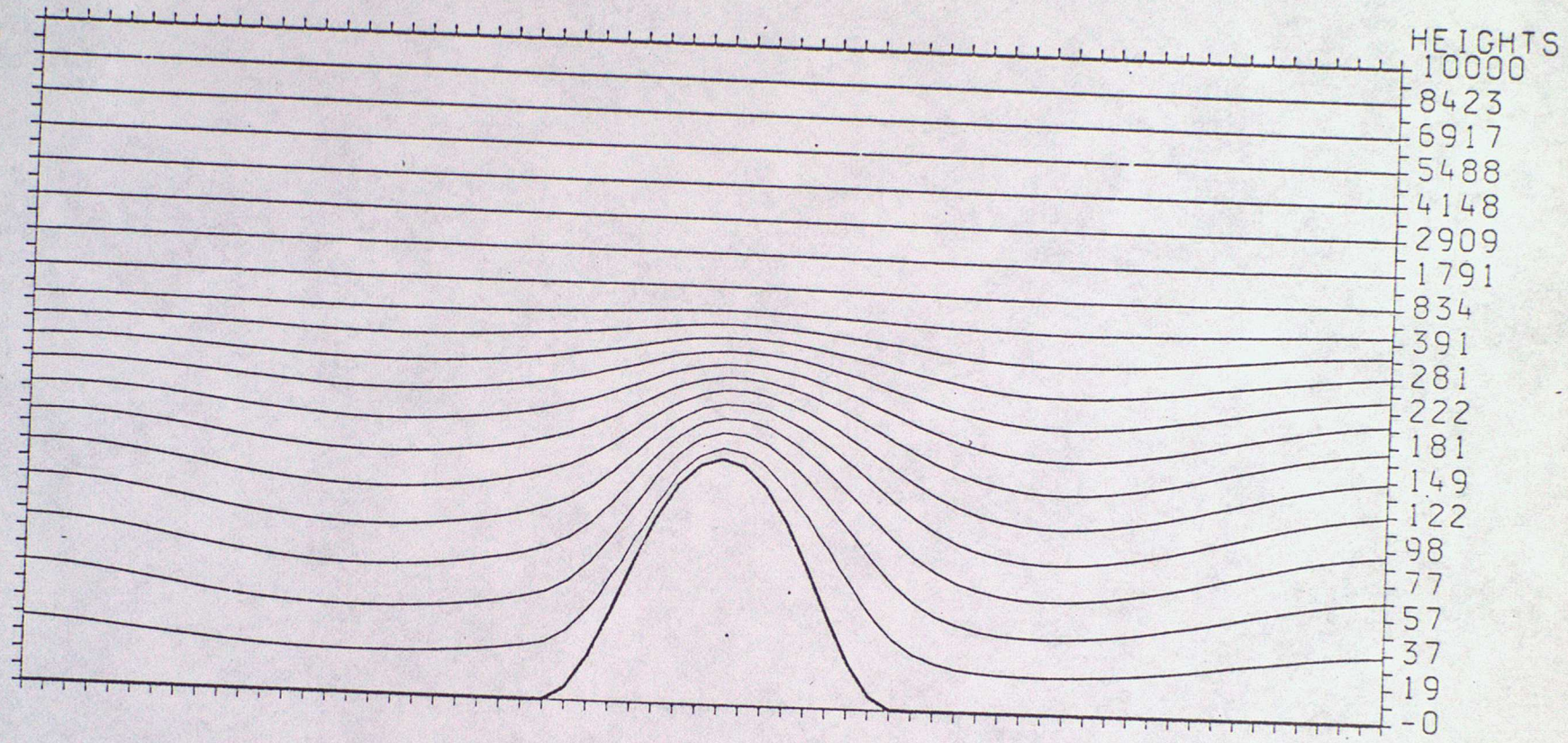
HEIGHTS
10000
8423
6917
5488
4148
2909
1791
834
391
281
222
181
149
122
98
77
57
37
19
-0

Fig 4.5

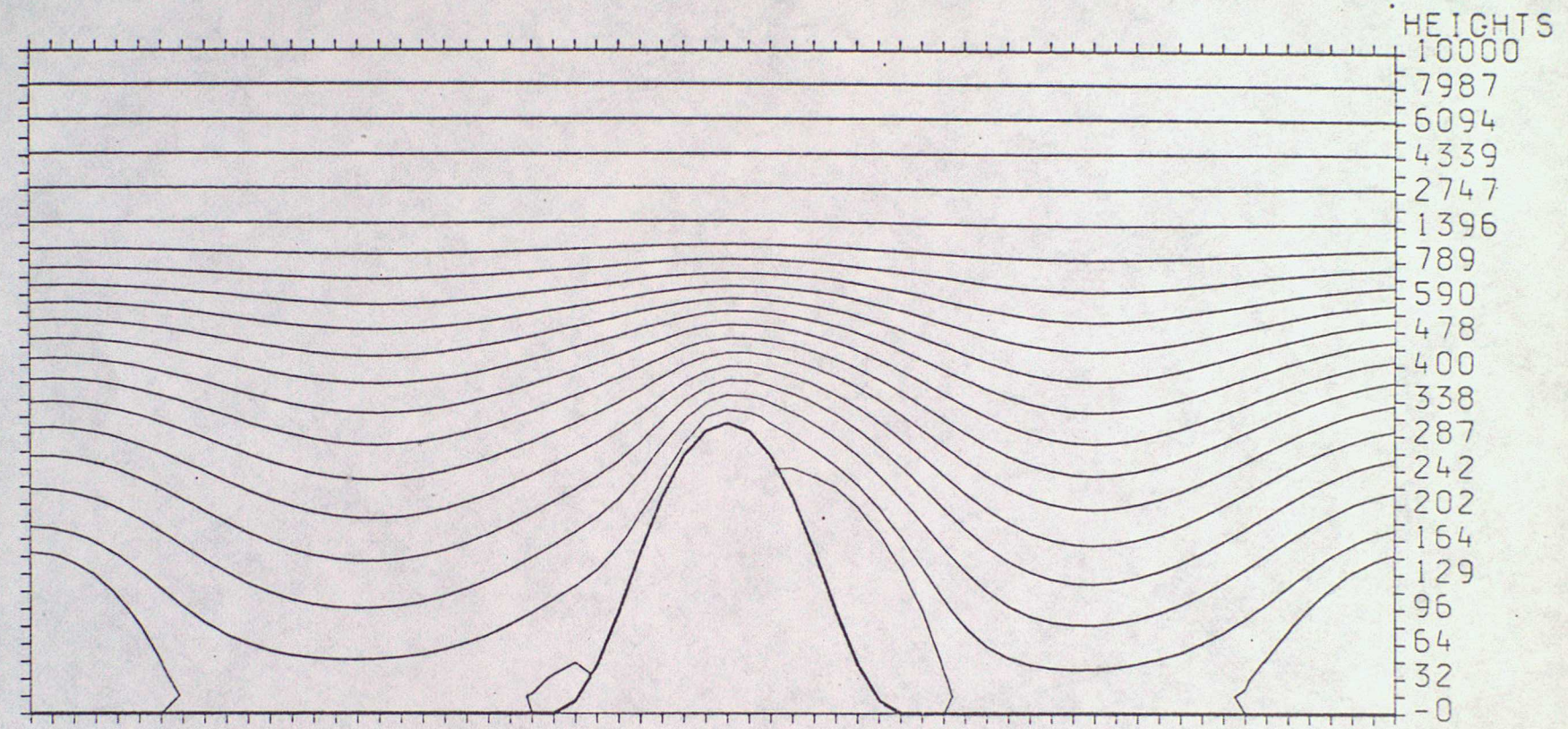
HEIGHTS
10000
7987
6094
4339
2747
1396
789
590
478
400
338
287
242
202
164
129
96
64
32
-0

Fig 049

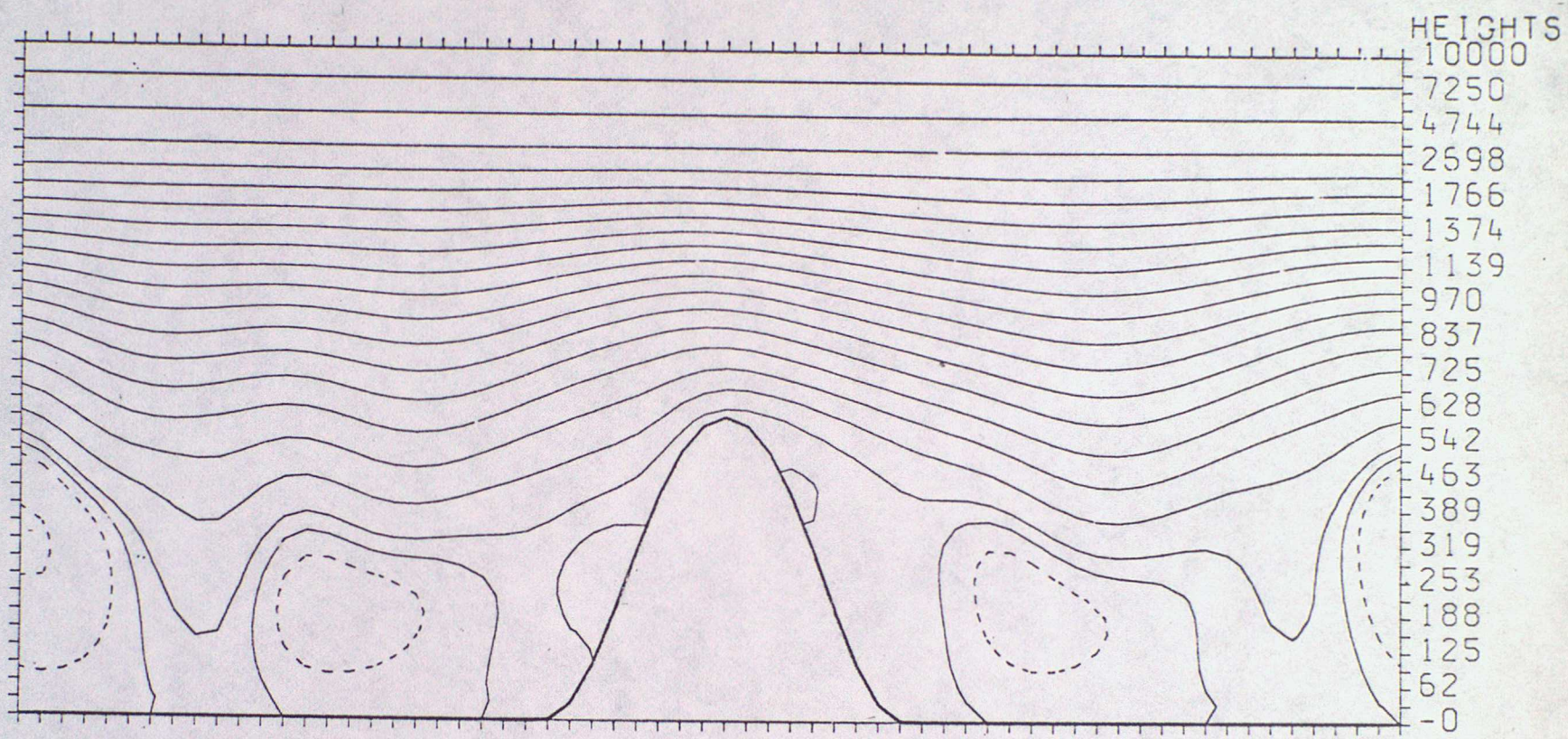
HEIGHTS
10000
7250
4744
2598
1766
1374
1139
970
837
725
628
542
463
389
319
253
188
125
62
-0

Fig 04h

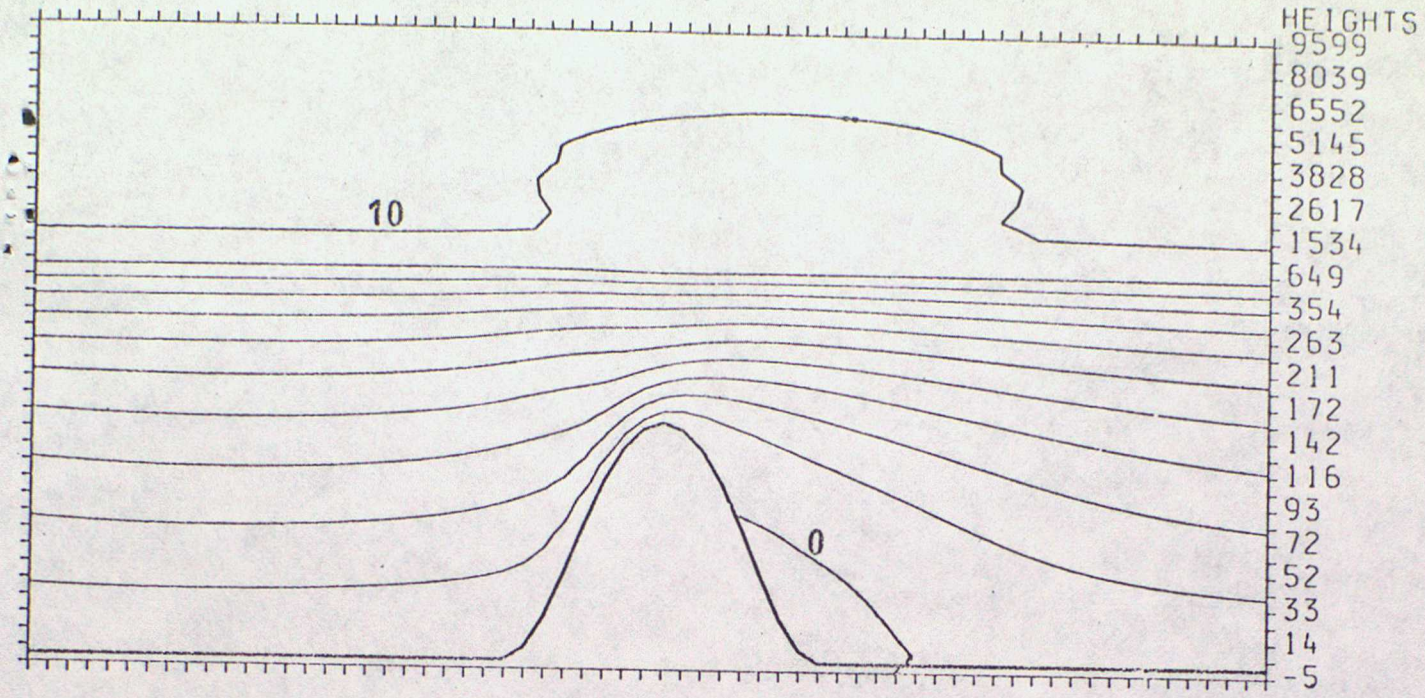
HEIGHTS
9599
8039
6552
5145
3828
2617
1534
649
354
263
211
172
142
116
93
72
52
33
14
-5
10
0

Fig 5a

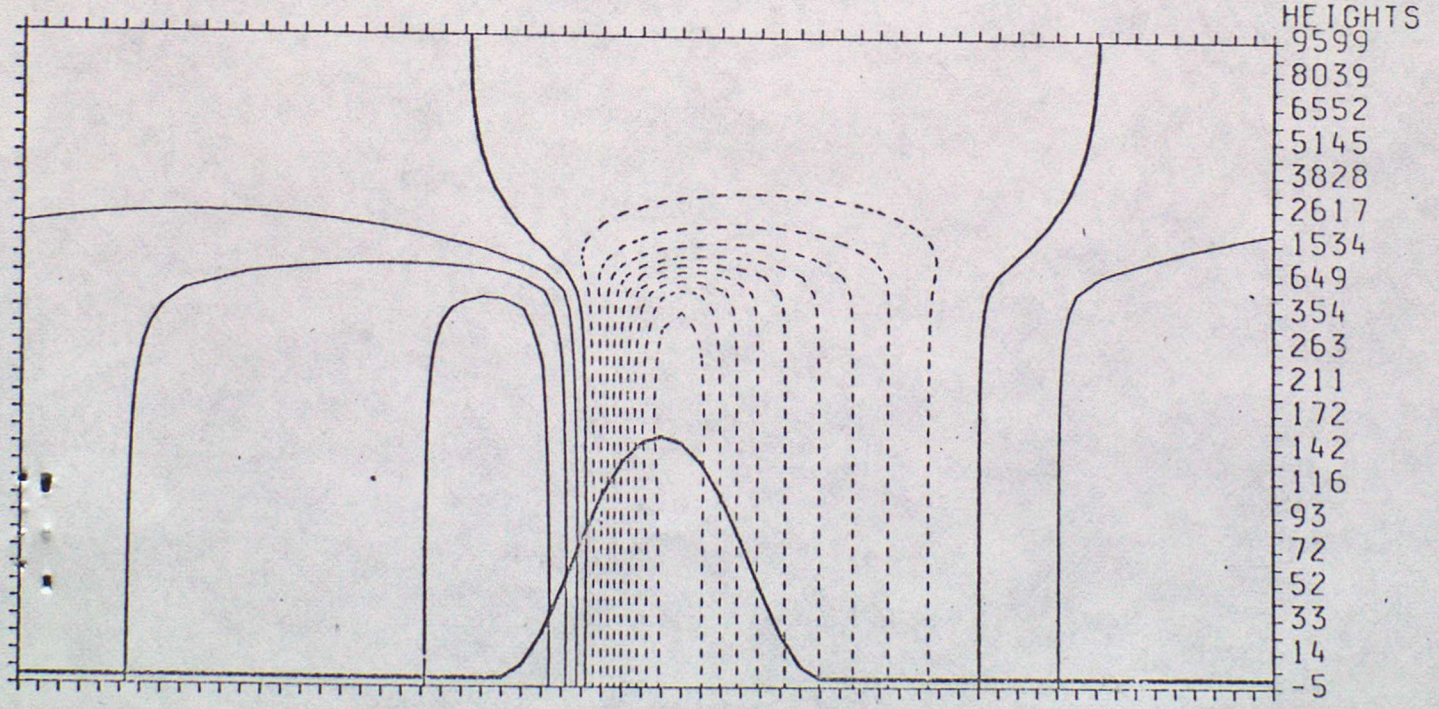
HEIGHTS
9599
8039
6552
5145
3828
2617
1534
649
354
263
211
172
142
116
93
72
52
33
14
-5

Fig 5b

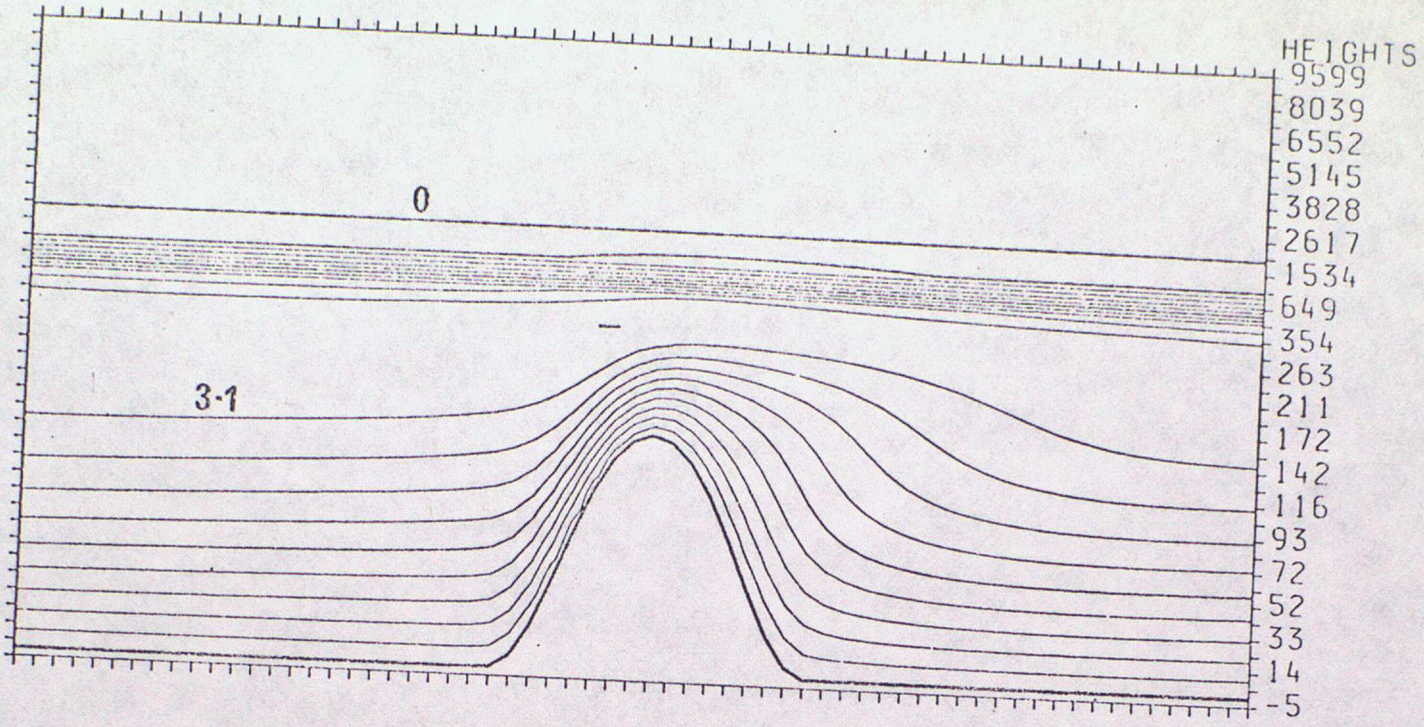
HEIGHTS
9599
8039
6552
5145
3828
2617
1534
649
354
263
211
172
142
116
93
72
52
33
14
-5
0
3-1

Fig 5c

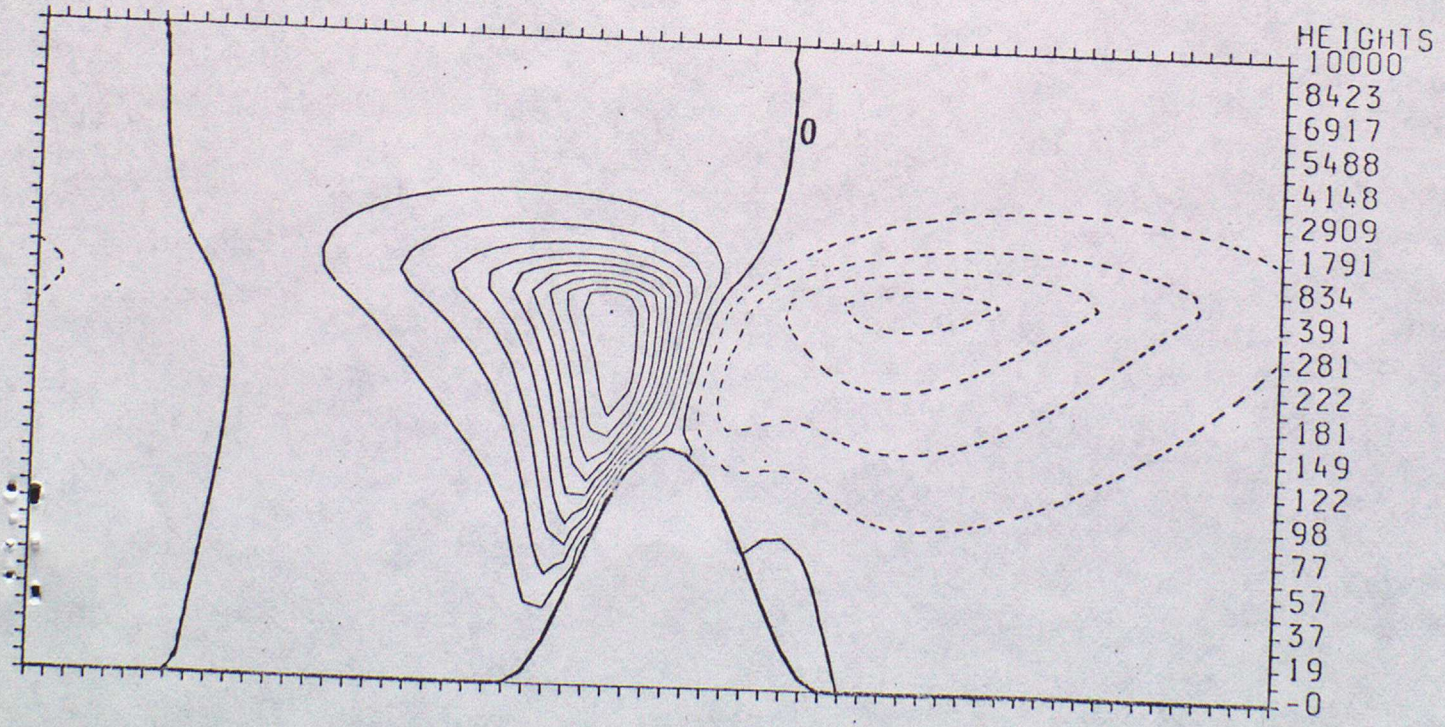
HEIGHTS
10000
8423
6917
5488
4148
2909
1791
834
391
281
222
181
149
122
98
77
57
37
19
-0
0

Fig 5d

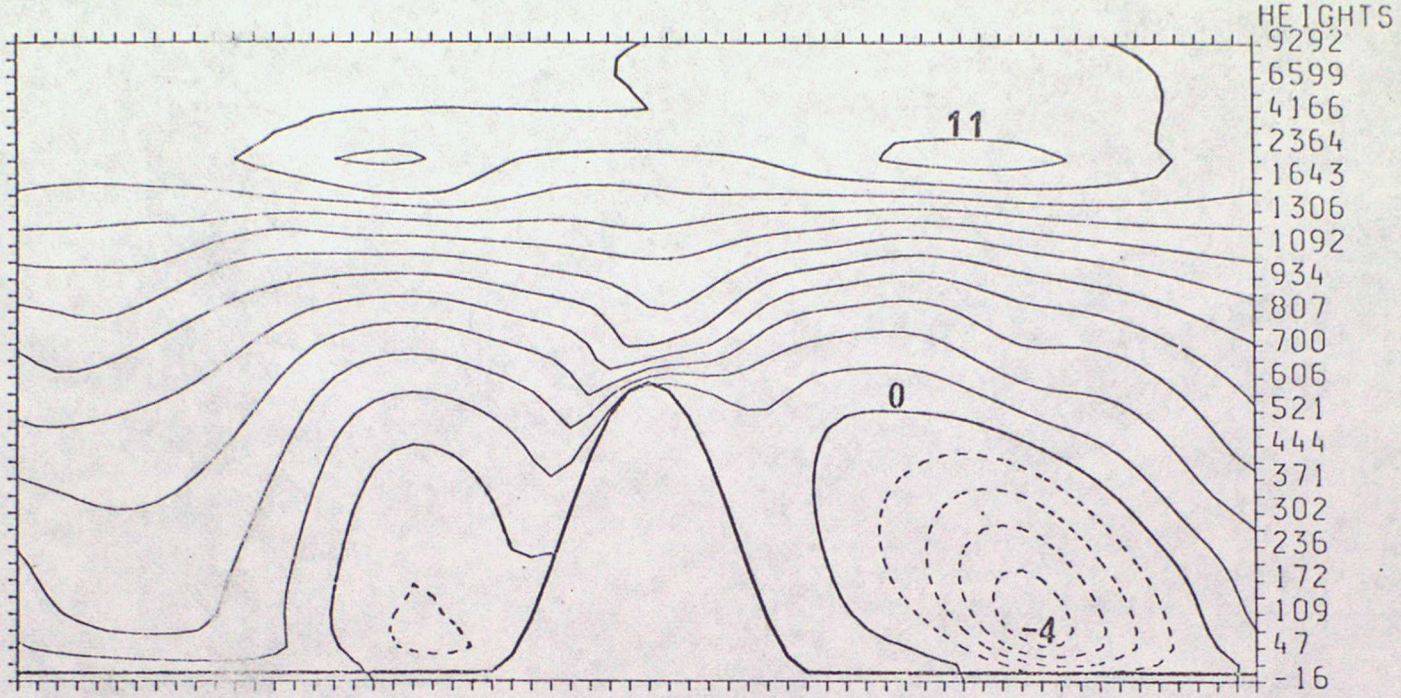
HEIGHTS
9292
6599
4166
2364
1643
1306
1092
934
807
700
606
521
444
371
302
236
172
109
47
-16
11
0
-4

Fig 6a

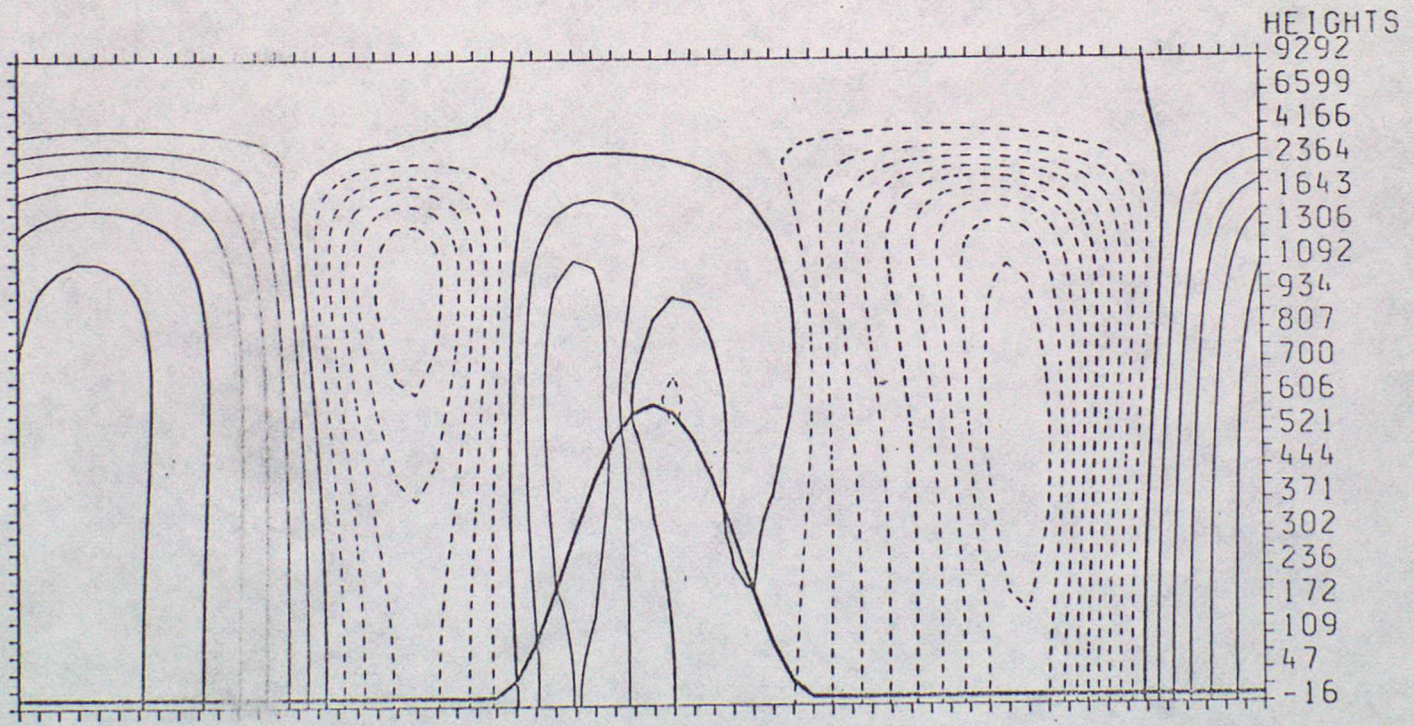
HEIGHTS
9292
6599
4166
2364
1643
1306
1092
934
807
700
606
521
444
371
302
236
172
109
47
-16

Fig 6b

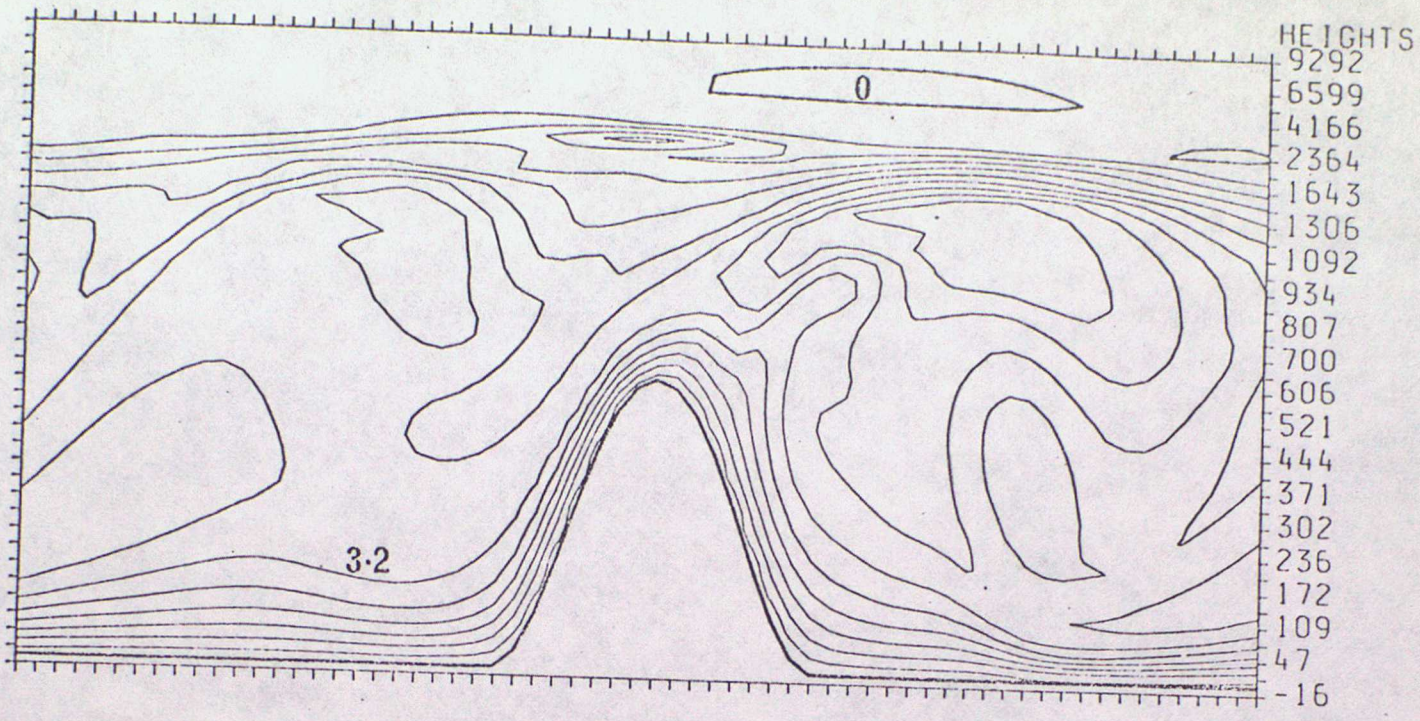
HEIGHTS
9292
6599
4166
2364
1643
1306
1092
934
807
700
606
521
444
371
302
236
172
109
47
-16
0
3·2

Fig 6c

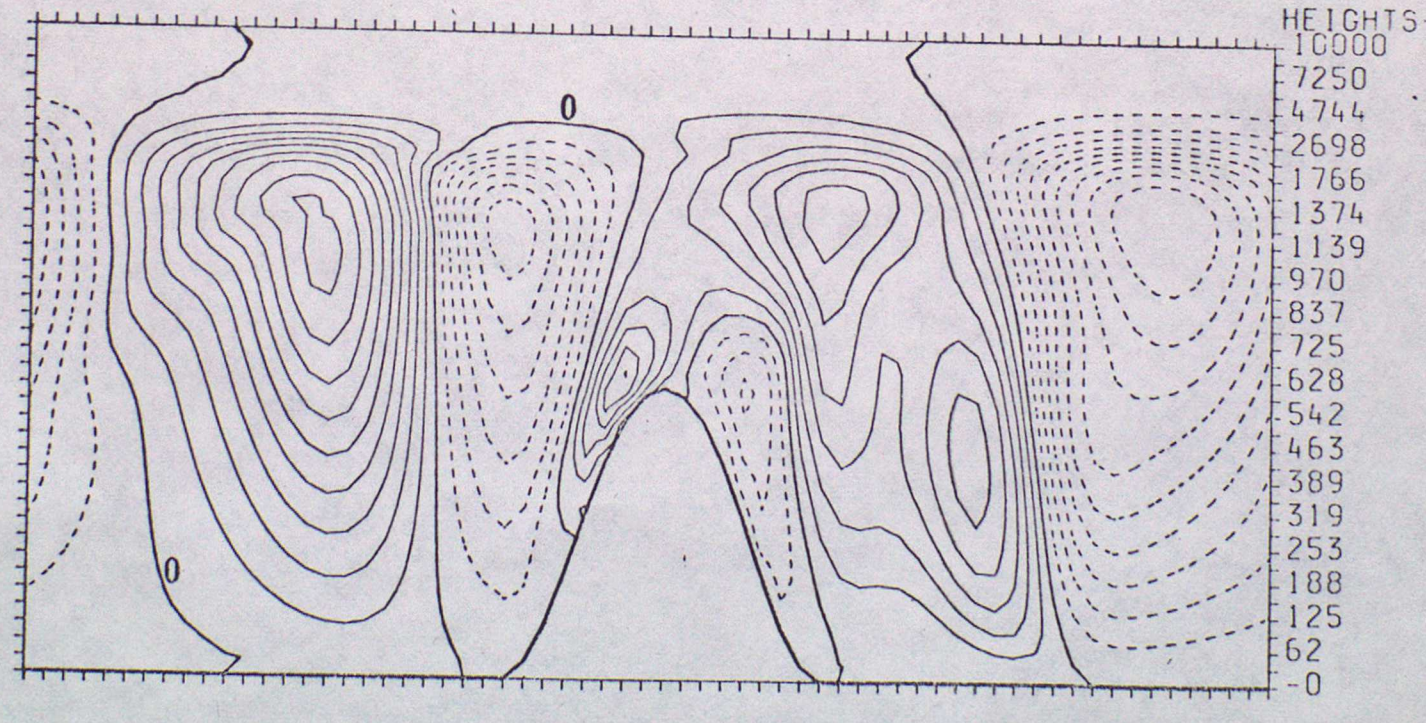
HEIGHTS
10000
7250
4744
2698
1766
1374
1139
970
837
725
628
542
463
389
319
253
188
125
62
-0
0
0

Fig 6d